Published in final edited form as:
Eur J Med Chem. 2014 September 12; 84: 476–490. doi:10.1016/j.ejmech.2014.07.050.

Novel 9′-substituted-noscapines: Synthesis with Suzuki cross-coupling, structure elucidation and biological evaluation

Elena Porcù[a,1], **Attila Sipos**[e,1], **Giuseppe Basso**[a], **Ernest Hamel**[b], **Ruoli Bai**[b], **Verena Stempfer**[c], **Antal Udvardy**[d], **Attila Cs. Bényei**[d,e], **Helmut Schmidhammer**[c], **Sàndor Antus**[f], and **Giampietro Viola**[a,*]

[a]Department of Woman's and Child's Health, Laboratory of Oncohematology, University of Padova, Via Giustiniani 2, Padova 35128, Italy

[b]Screening Technologies Branch, Developmental Therapeutics Program, Division of Cancer Treatment and Diagnosis, Frederick National Laboratory for Cancer Research, National Cancer Institute, National Institutes of Health, Frederick, MD 21702, USA

[c]Department of Pharmaceutical Chemistry, Institute of Pharmacy and Center for Molecular Biosciences Innsbruck, University of Innsbruck, Austria

[d]Department of Physical Chemistry, University of Debrecen, Hungary

[e]Department of Pharmaceutical Chemistry, Medical and Health Science Center, University of Debrecen, Hungary

[f]Department of Organic Chemistry, University of Debrecen, Hungary

Abstract

Tubulin is a major molecular target for anticancer drugs. The dynamic process of microtubule assembly and disassembly can be blocked by various agents that bind to distinct sites on tubulin, usually its β-subunit. Among the antimitotic agents that perturb microtubule dynamics, noscapinoids represent an emerging class of agents. In particular, 9′-bromonoscapine (EM011) has been identified as a potent noscapine analog. Here we present high yielding, efficient synthetic methods based on Suzuki coupling of 9′-alkyl and 9′-arylnoscapines and an evaluation of their antiproliferative properties. Our results showed that 9′-alkyl and 9′-aryl derivatives inhibit proliferation of human cancer cells. The most active compounds were the 9′-methyl and the 9′-phenyl derivatives, which showed similar cytotoxic potency in comparison to the 9′-brominated derivative. Interestingly these newly synthesized derivatives did not induce cell death in normal human lymphocytes, suggesting that the compounds may be selective against cancer cells. All of these derivatives, except 9′-(2-methoxyphenyl)-noscapine, efficiently induced a cell cycle arrest in the G2/M phase of the cell cycle in HeLa and Jurkat cells. Furthermore, we showed that the most active compounds in HeLa cells induced apoptosis following the mitochondrial pathway with the activation of both caspase-9 and caspase-3. In addition, these compounds significantly reduced the expression of the antiapoptotic proteins Mcl-1 and Bcl-2.

*Corresponding author. Giampietro.viola.1@unipd.it, (G. Viola).
[1]Equal contributing authors.

Keywords

Noscapine; Antimicrotubule agents; Apoptosis; Cell cycle arrest; Suzuki reaction

1. Introduction

Antimitotic agents, primarily of natural origin, are a class of compounds that have been used for the treatment of a variety of malignancies for many years. Although they are sometimes considered “old chemotherapeutics” with respect to current anticancer approaches [1,2], at the present time they still represent valuable drugs that retain high scientific interest. Their impressive success in patients is due to their potent antiproliferative effects and to their particular mechanism of action of altering microtubule dynamics, whether their detailed mechanism of action involves inhibition of tubulin assembly (vinca alkaloids, eribulin, estramustine, drug–antibody complexes with dolastatin 10 and maytansine analogues) or inhibition of microtubule disassembly (taxoids, epothilones). The importance of microtubules in mitosis and cell division, as well as the clinical success of microtubule targeting drugs, has made these dynamic organelles one of the most attractive targets for anticancer therapy [3]. In 1997, Ye et al. [4] discovered the anti-cancer effect of noscapine [**1**, (−)-α-noscapine, (*S*)-6,7-dimethoxy-3-((*R*)-4′-methoxy-6′-methyl-5′,6′,7′,8′-tetrahydro[1,3]dioxolo-[4,5]isoquinolin-5′-yl)isobenzofuran-1(*3H*)-one], formerly known as narcotine (Fig. 1), a phthalide isoquinoline alkaloid constituting 1–10% of the alkaloid content of opium. The antimitotic activity of noscapinewas characterized, and it was demonstrated that the compound could inhibit tubulin assembly. These workers therefore embarked on an intensive search for more potent analogues of noscapine [4,5].

Most importantly, 9′-bromonoscapine (**2**, EM011) was patented [6], characterized, and introduced into clinical trials against non-Hodgkin's lymphoma and chronic lymphocytic leukemia. A few other 9′-substituted noscapine derivatives were reported recently [7–10]. For instance 9′-nitronoscapine was found to be active against drug-resistant ovarian cancer and T-cell lymphoma cells [8], and its reduced congener, 9′-aminonoscapine, has good activity as a tubulin inhibitor [10].

Considering the increased cytotoxic activity of the 9′-bromo derivative of **1** as compared with the parent molecule, it is important to know whether the substitution of the phtalideisoquinoline backbone in position 9′ contributes to a conformational change. Besides that, it is known from previous reports that phtalideisoquinoline derivatives are sensitive to acidic or basic media, and in numerous cases epimerization occurs [11,12]. Therefore, it was considered important to unambiguously determine whether or not there is an epimerization reaction during the relatively harsh bromination procedure. Thus, we obtained crystals of 9′-bromonoscapine (**2**) for X-ray crystallography and investigated the circular dichroism of compound **2** in solution. In addition, 9′-bromonoscapine (**2**) prepared by a modified procedure, was identified as a starting agent for the synthesis of new analogues through the application of modern Pd-catalyzed cross-coupling reactions (Scheme 1) [13]. These new 9′-alkyl and 9′-arylnoscapines were evaluated for their antiproliferative and anti-tubulin properties, as well as their apoptotic mechanism of action.

2. Chemistry

The literature procedure for the preparation of 9′-bromonoscapine (**2**) was published in 2003 by Zhou et al. [7]. This procedure began with noscapine free base and used the 48% HBr-bromine water reactant mixture for the bromination of noscapine at position 9′. Afterward, the alkalinization of the reaction mixture was performed with cc. NH_3 solution. The filtration of the crude product was followed by recrystallization from 96% ethanol. In our hands, this procedure gave rise to the desired 9′-bromonoscapine in a considerably lower yield (<10%), so we optimized the procedure in several steps. The application of extraction after filtration of the aqueous phase of the crude product resulted in a significant amount of off-white product that was a mixture of 9′-bromonoscapine (**2**) and a large amount of unreacted noscapine (**1**). Recrystallization from 96% ethanol yielded only a very small amount of **2**. The separation of noscapine **1** and its bromo derivative **2** was also attempted several times by column chromatography, but the highly similar retention times of the two compounds prevented their separation, even after trying many different mobile phases. 9′-Bromonoscapine (**2**) was prepared by a modified procedure [7] and used as a starting material for the synthesis of new analogues through the application of modern Pd-catalyzed cross-coupling reactions.

This approach was found to be superior as solvation required less HBr, and this led to an increase in product purity and yield. The yield was further improved by processing the mother liquor and using less base for the neutralization step. The concentration of the mother liquor resulted in a significant amount of a light yellow residue that was found to be 9′-bromonoscapine (**2**) containing a small amount of noscapine impurity. These modifications combined afforded a total yield of 50% on average. The pure 9′-bromonoscapine (**2**) we obtained, confirmed by ^{1}H NMR, showed a higher melting point than the reported value (174–175 °C instead of 169–170 °C). The 9′-bromonoscapine (**2**) obtained was used as a starting agent for its transformation by the application of modern Pd-catalyzed cross-coupling reactions (Suzuki reaction) into new 9′-noscapine derivatives. The application of Suzuki cross-coupling reaction in the synthesis and derivatization of alkaloids is an excellent choice for the formation of new C–C bonds. For example, substitutions in morphinans and aporphinoids were successfully realized at different positions of the two alkaloid backbones [14–16]. The first tested protocol with **2** was adapted from these earlier procedures using K_2CO_3 as a base and $Pd[P(Ph)_3]_4$ as the Pd-source combined with ligands. As summarized in Table 1, this combination of reagents and reaction conditions (heating at 90 °C for 2 h) led to 4–12% percent yields after isolation by means of column chromatography. After testing other generally used reagents and conditions, we found no significant improvement with these common coupling methodologies. After examining the single crystal structure of compound **2** (*vide infra*), especially the steric hindrance in the proximity of the bromine substituent, we turned to methods developed for the cross-coupling of hindered aromatic bromides [17]. The application of $Pd(OAc)_2$ as the Pd-source, K_3PO_4 as the base and XPhos, a specific biphenyl phosphine, made possible the isolation of the desired products **3–8** in significantly higher yields (Table 1).

2.1. Structural analysis of 9′-bromonoscapine (2) and Suzuki products 3–8

The structure of compound **2** in solution was investigated with the use of circular dichroism (CD). In Fig. 2 (Panel A) the CD spectra of parent compound **1** and its brominated congener **2** are presented. The spectrum of (−)-α-isomer **1** shows Cotton effects around 320 and 225 nm. These data are in accordance with the most relevant and detailed evaluation of the circular dichroism characteristics of phthalide isoquinoline alkaloids by Snatzke et al. [18]. As concluded in this fundamental work, the configuration of the C5′ asymmetric centre could be associated with Cotton effects at around 290 (^1L_B transition) and 205 nm (^1B aromatic transition), while the data related to the configuration of the C3 carbon appear in the regions of 320 and 225 nm (aromatic transitions). Comparing the CD spectra obtained for compounds **1** and **2**, it can be unambiguously stated that the characteristics, the types and the positions of Cotton-effects confirm the high conformational similarity between the two molecules. On the basis of the X-ray crystal structure, the torsion angle between the H3–C3–C5′–H5′ atoms can be measured (Fig. 3, panel A). These data are considered an efficient indicator for showing the relative positions of the tetrahydroisoquinoline and isobenzofuranone ring systems of the phthalide isoquinoline derivatives. The angle for natural noscapine base (**1**) was reported to be −66° [19]. Interestingly, the protonation of the tertiary amino function (formation of noscapine hydrochloride) is followed by a remarkable conformational change characterized by the important torsional angle of +78°for the H3–C3–C5′–H5′ atomic connections [20]. As presented in Fig. 3 (panel B), the protonation evokes a significant twisting of the isobenzofuranone moiety relative to the tetrahydroisoquinoline group. The modified synthesis of 9′-bromonoscapine (**2**) allowed us to obtain crystals of the compounds appropriate for single crystal X-ray structural analysis (CCDC deposition # 955643) (Fig. 3, panel C). It was determined that the indicative torsion angle between H3–C3–C5′–H5′ for the 9′-bromonoscapine was −80.1°. A recent study on the three dimensional chemical space of a pharmacophore model for noscapinoids [21] allows us to determine that the relative positions of hydrogen bond acceptor O1′ and C7–OCH_3 oxygen atoms and the hydrophobic C4′–OCH_3 and C6–OCH_3 methyl centres are within 1.2 Å of maximal distance. This was done after performing the overlay of the X-ray structures of the free bases of noscapine (**1**) and 9′-bromonoscapine (**2**) by overlaying the structures of both the tetrahydroisoquinoline and isobenzofuranone ring systems. In order to prove that the Suzuki cross-coupling conditions did not lead to epimerization of the original phthalide isoquinoline structure (i.e., that the conformations of the synthesized compounds were similar to the pharmacologically promising precursor **2**), the circular dichroism spectra of compounds **3–8** were recorded. The α-isomers of phthalide isoquinoline alkaloids show Cotton effects typically around 320 and 225 nm. It can be concluded from the set of CD spectra presented in Fig. 2 (panel B), that in these regions the spectra show similar characteristics, which is a proof of the retention of configuration at the two chiral centers.

3. Results and discussion

3.1. Evaluation of antiproliferative activity

The newly synthesized noscapine derivatives, in comparison with reference compound **2**, were tested for their antiproliferative activity in a panel of human cancer cell lines. As shown in Table 2, 9′-aryl derivatives **4** and **5** and the 9′-alkyl derivative **3** present higher

values of IC_{50} respect to with 9′-bromonoscapine (**2**). Generally less active than **2**, the three methoxyphenyl derivatives **6–8**, as well as the 9′-alkyl derivative **9**, showed similar potencies to each other. To obtain more insight into the potential cytotoxic activity of these new compounds for normal human cells, they were assayed *in vitro* against peripheral blood lymphocytes (PBL) from healthy donors (Table 3). All the compounds were ineffective in resting lymphocytes, having IC_{50} values over 200 μM, in well agreement with previous reports [5,7]. Only some compounds (**2, 4** and **6**) proved cytotoxic in PHA-stimulated PBL, but only at higher concentrations (generally, 5–30 fold higher) than against the lymphoblastic cell lines Jurkat and CCRF-CEM. Together, these data suggest these compounds may have cancer cell selective killing properties.

3.2. Inhibition of tubulin polymerization and colchicine binding

The series of new noscapine analogues was first evaluated for potential inhibition of tubulin assembly in comparison with the potent colchicine site agent combretastatin A-4 (CA-4), using a GTP- and glutamate-dependent polymerization assay that measured extent of assembly after 20 min at 30 °C (Table 4) [22]. It was quickly apparent that, while some activity was observed with several of the noscapine analogues, they were far less potent than CA-4, which yielded an IC_{50} value of 1.2 μM. In fact, when concentrations up to 400 μM were evaluated, an IC_{50} value was obtained only with compound **5**. The inhibition observed with **5** (IC_{50}, 120 μM) was 100-fold weaker than the inhibition observed with CA-4. However, besides IC_{50} values based on inhibition of the extent of assembly, it is also possible to change the parameter measured from the extent to the rate of assembly [22–24]. In our experience, this has the effect of reducing the IC_{50} value for compounds 2–4-fold, thus permitting measurements of IC_{50}'s for weakly active compounds and, potentially, for compounds that induce aberrant polymer formation at higher concentrations, which is generally associated with turbidity development that can only be distinguished from "normal" assembly by electron microscopy [25,26]. Our concentration studies with the noscapine analogues did not provide any evidence for an aberrant assembly reaction, since we only observed progressive inhibition, albeit very weak. In addition, it should be noted that the typical microtubule assembly curve, as measured by turbidimetry, has a sigmoidal shape. We therefore measured the maximum rate of assembly at the inflection points of the turbidity curves. This resulted in our obtaining 3-fold reductions in the IC_{50} values for CA-4 (0.44 μM) and **5** (45 μM), but, in addition, we obtained maximum rate IC_{50} values for two compounds (**3** and **7**) (Table 4). Only, **2, 4**, and **6** failed to yield rate IC_{50} values.

Because noscapine has structural similarity to colchicine, it was evaluated without success as a potential inhibitor of [^{3}H]colchicine binding to tubulin [4]. With most active colchicine site inhibitors, we have been able to demonstrate significant inhibition of the binding of [^{3}H]colchicine to tubulin, with tubulin at 1 μM and colchicine and the inhibitor at 5 μM. This is shown in Table 4 for CA-4, although few compounds are as potent as CA-4 in inhibiting this reaction. With the noscapine analogues, in agreement with the findings with noscapine, [4] in a preliminary experiment we found no significant activity when they were added to the reaction mixture at 5 μM(data not shown). However, we decided to evaluate the compounds for potential inhibition at 500 μM (Table 4).We did observe inhibition reasonably concordant with the effects on tubulin assembly. Thus, the best inhibition was

observed with **5**, and the worst with the three compounds that had assembly rate IC_{50} values over 400 μM (**2, 4**, and **6**).We should note here that this assembly assay uses reaction conditions that strongly stabilize the colchicine binding activity of tubulin [16]. Nevertheless, we generally measure inhibition of colchicine binding at short reaction times, such as 10 min, when the reaction is 40–60% complete, because we have found that inhibition by weakly active compounds is maximal at shorter incubation times [27]. This is probably because most colchicine site agents dissociate from tubulin much more rapidly than colchicine itself [27,28]. Consequently, once bound, [^{3}H]colchicine in effect locks other agents out of the binding site. Under the reaction conditions used here, the half-life of the colchicine–tubulin complex is about 24 h [28]. The difference in reaction conditions and incubation time probably explains the limited effects reported for noscapine on the binding of [^{3}H] colchicine to tubulin [4]. We should note, however, that a recent report [29] described inhibition of colchicine binding, measured by inhibition of the fluorescence that occurs when colchicine binds to tubulin [30], by 9′-bromonoscapine (**2**), although noscapine (**1**) itself had no activity at the highest concentration examined (100 μM).

3.3. Effects of 9′-noscapine derivatives on the cellular microtubule network

We investigated the effects of the new derivatives on the cytoskeletal microtubule and microfilament networks by immunofluorescence in HeLa cells. As shown in Fig. 4, the microtubule network exhibited normal arrangement and organization in HeLa cells in the absence of drug treatment. In contrast, 24 h of exposure to compounds **2, 3** or **7** at 25 μM caused extensive microtubule rearrangement, with induction of spherical morphology in 70–80% of the cells. In addition, the treatment also induced mitotic arrest, characterized at the concentrations and time studied, by an increase in the number of cells with typical bipolar spindles with chromosomes arranged along the metaphase plate. We also observed abnormal microtubule spindles with astral or multipolar configurations as well as a disorganized or spherical arrangement of chromosomes. In good agreement with microtubule rearrangement, we also observed PCM1 alteration, after treatment of cells with the new compounds (effects of compounds **2, 3** and **5** shown in Fig. 5). PCM1 is a pericentriolar protein involved in recruiting proteins necessary for centrosome replication, and it dynamically fluctuates during the cell cycle. Late in G2, the protein dissociates from the centrosome remaining dispersed throughout the cell during mitosis. The mechanism is cell cycle dependent, with PCM1 aggregates disassembling during mitosis and reassembling in interphase [31,32].

As shown in Fig. 5, PCM1 staining revealed an accumulation of the pericentriolar material in some treated cells, similar to the effects observed after treatment with nocodazole and other antimitotics [33]. Moreover, cells arrested in mitosis showed the characteristic rounded shape, and PCM1 was scattered and dispersed throughout the cell. The derivatives induced a depletion of PCM1 function, affecting its localization and the organization of cell cycle machinery, resulting in microtubules anchoring to the centrosome. The derivatives also induced a change in cell morphology detectable by staining with phalloidin (Fig. 5). Actin filaments were intact but disorganized as compared with the control cells, contributing to impairment of cell organization.

3.4. 9′-Noscapine derivatives induce G2/M arrest of the cell cycle

The effects of a 24 h treatment with different concentrations of compounds **2**–7 on cell cycle progression in HeLa (Fig. 6) and Jurkat cells (Fig. 7), were determined by flow cytometry. All compounds, except **6**, caused a significant G2/M arrest in a concentration-dependent manner in both cell lines, with the new compounds having effects essentially identical to those observed with the reference compound **2**. In HeLa cells (Fig. 6), the rise in G2/M cells occurred maximally at a concentration between 10 and 25 μM, while at higher concentrations more than 80% of the cells were arrested in G2/M. A similar behavior was observed with the Jurkat cells (Fig. 7), but, except with compound **2**, maximal effects required higher compound concentrations. As would be expected, the cell cycle arrest in G2/M phase was accompanied by a commensurate reduction in cells in the other phases of the cell cycle. We also examined several of the compounds, in comparison with CA-4, in human Burkitt lymphoma CA46 cells since this cell line generally yield a very high mitotic index when treated with antitubulin agents. Compounds **3** and **7** yielded IC_{50} values of 18 ± 8 μM and 20 ± 4 μM, respectively (the contemporaneously obtained value for CA-4 was 20 ± 7 nM). At five times the IC_{50} concentrations, there was over 80% G2/M cells with all three compounds. Morphological examination of parallel cultures stained with Giemsa yielded mitotic indices of 46% with CA-4, 38% with compound **3**, and 28% with compound **7** indicating that they acted like antitubulin agents. We next studied the effects of compounds **2–5**, on alterations in the expression of proteins that regulate cell division. The cdc2/cyclin B complex controls both entry into and exit from mitosis. Phosphorylation of cdc2 on Tyr15 and phosphorylation of cdc25c phosphatase on Ser216 negatively regulate the activation of the cdc2/cyclin B complex [34–36]. Thus, dephosphorylation of these proteins is needed to activate the cdc2/cyclin B complex. Cdc25c is a major phosphatase that dephosphorylates the site on cdc2 and auto-dephosphorylates itself. Phosphorylation of cdc25C directly stimulates both its phosphatase and autophosphatase activities, a condition necessary to activate cdc2/cyclin B on entry of cells into mitosis [34–36]. As shown in Fig. 8 in HeLa cells, treatment with **3, 4** or **5** at 25 μM for 24 or 48 h caused an increased expression of cyclin B at 24 h, in particular for compounds **5**, followed by its disappearance at 48 h. Similarly, slower migrating forms of phosphatase cdc25C appeared at 24 h following treatment with **4** or **5**, indicating changes in the phosphorylation state of this protein, while at 48 h with these compounds, as well as compound **2**, the expression of cdc25c strongly decreased. We also observed a dramatic reduction in the expression of the phosphorylated form of cdc2 (Tyr15) with all tested compounds. We also examined the effect of the new derivatives on the expression of aurora kinase A and its phosphorylated form at T288 since the phosphorylation of aurora kinase A is a hallmark of the G2/M phase [37]. As shown in Fig. 8, aurora kinase levels increased after a 24 h treatment with compounds **3, 4** and **5**, but not **2**. Altogether these data suggest, as did the immunofluorescence studies, that the observed G2/M arrest was not due to a defect in G2 to M phase progression but instead was caused by aberrant execution of mitosis.

Prolonged mitotic arrest can lead to DNA damage [38,39]. We identified DNA damage through the detection of the phosphorylated histone γ-H2A.X. Compounds **3, 4** and **5** induced a marked increase in the expression of γ-H2A.X after a 24 h treatment, while a similar increase was observed after 48 h with compound **2**, suggesting that these compounds

induce major DNA damage during mitotic arrest that could contribute to their antiproliferative activity.

3.5. 9′-Noscapine derivatives induce apoptosis

To characterize the mode of cell death induced by these compounds, a biparametric cytofluorimetric analysis was performed using PI, which stains DNA and enters only dead cells, and fluorescent immunolabeling of the protein annexin-V, which binds to PS in a highly selective manner [40]. Compounds **2–5** were incubated with HeLa cells for 24 or 48 h and then stained with the two dyes. Dual staining with annexin-V and with PI permits discrimination between live cells (annexin-V^-/PI^-), early apoptotic cells (annexin-V^+/PI^-), late apoptotic cells (annexin-V^+/PI^+) and necrotic cells (annexin-V^-/PI^+). As depicted in Fig. 9 (Panels A–E), the treated HeLa cells showed an accumulation of annexin-V positive cells in comparison with the control, in a concentration and time-dependent manner. In good agreement with MTT data, the reference compound **2** was slightly more active than the other three compounds.

3.6. 9′-Noscapine derivatives induce apoptosis through the mitochondrial pathway

Mitochondria play an essential role in the propagation of apoptosis [41]. It iswell established that, at an early stage, apoptotic stimuli alter the mitochondrial transmembrane potential ($\Delta\psi_{mt}$) [42]. $\Delta\psi_{mt}$ was monitored by the fluorescence of the dye JC-1. As shown in Fig. 10 (Panels A–D), compounds **2–5** induced a time and concentration-dependent increase in the proportion of cells with depolarized mitochondria. Mitochondrial membrane depolarization is associated with mitochondrial production of ROS [43]. Therefore, we investigated whether ROS production increased after treatment with **2–5**. We analyzed the production of ROS by flow cytometry utilizing the fluorescence indicator H_2-DCFDA. The results presented in Fig. 11 (Panels A–D) show that all the tested compounds induced the production of significant amounts of ROS in comparison with control cells, which agrees with the previously described dissipation of $\Delta\psi_{mt}$. Altogether, these results indicate that these compounds induced apoptosis through the mitochondrial pathway in good agreement with previous reports [44–46].

3.7. Effect of 9′-alkyl and 9′-arylnoscapines on caspase activation

The activation of caspases plays a central role in the process of apoptotic cell death [47]. Synthesized as proenzymes, caspases are themselves activated by specific proteolytic cleavage reactions. Caspases-2, -8, -9, and -10 are termed initiator caspases and are usually the first to be activated in the apoptotic process. Following their activation, they in turn activate effector caspases, in particular caspase-3 [48]. As shown in Fig. 12 (Panel A), all tested compounds induced proteolytic cleavage of caspase-9 and caspase-3, in good agreement with the mitochondrial depolarization described above. The DNA repair enzyme PARP is cleaved by caspase-3 from its full length 116 kDa form to an inactive 85 kDa form. We also observed that PARP cleavage was detectable after 24 h and 48 h treatments. Altogether, these results showed that apoptosis induced by the 9′-noscapine derivatives was caspase-dependent and followed the intrinsic (mitochondrial) pathway. These findings are in good agreement with those of Aneja et al. who found that 9′-bromonoscapine induces

mitochondrial depolarization followed by caspasedependent apoptosis in both human prostate cancer cells and leukemia cells [49,50].

3.8. Effect on proapoptotic proteins and IAP expression

There is increasing evidence that regulation of the Bcl-2 family proteins shares the signaling pathways induced by antimicrotubule compounds [44]. Several pro-apoptotic family proteins (e.g., Bax, Bid, Bim and Bak) promote the release of cytochrome *c*, whereas anti-apoptotic members (Bcl-2, Bcl-XL and Mcl-1) are capable of antagonizing the pro-apoptotic proteins and preventing the loss of mitochondrial membrane potential [44]. As shown in Fig. 12 (Panel B), after a 24 h treatment, Bcl-2 expression was reduced with compounds **2** and **3**, but not with compounds **4** and **5**. After a 48 h treatment, however. Bcl-2 expression was decreased with all four compounds (**2–5**). The pro-apoptotic protein Bax was essentially unchanged after either 24 or 48 h treatments. Mcl-1 is an antiapoptotic member of the Bcl-2 family, and recently it was reported that sensitivity to antimitotic drugs is regulated by Mcl-1 levels [51,52]. As shown in Fig. 12 (Panel B), the Mcl-1 band was strongly reduced after the 24 h treatment with compounds **2, 3** and **4**, but not **5**. After the 48 h treatment, the Mcl-1 band disappeared with all four compounds. It has recently emerged that Mcl-1 acts as a controller of the apoptotic timing response during mitotic arrest [51,52]. When Mcl-1 levels fall, Bak and Bax form pores in the mitochondrial membrane, resulting in the release of cytochrome *c*, mitochondrial depolarization and caspase activation that ultimately lead to apoptosis [52].

4. Conclusion

We devised an efficient new synthesis for noscapine derivatives modified at position 9′, using Suzuki cross-coupling, a specific palladium-catalyzed carbon–carbon bond formation reaction, on the phthalide isoquinoline backbone. The ligands examined here were chosen to study the general utility of the reaction and, equally importantly, to obtain new, potentially cytotoxic noscapine derivatives. As shown above, 9′-bromonoscapine (**2**) has a very similar conformation in solid phase as the noscapine free base (**1**). This suggests that cytotoxic activity is a consequence of electronic rather than structural effects.

We also showed that the new 9′-substituted noscapines shared common properties with the lead compound **2** and are efficacious as antiproliferative agents in different cancer cell lines. It is worthwhile to note that our compounds present higher cytotoxicity in comparison to other noscapine derivatives recently synthesized such as 6′-substituted [53] but similar to that of a series of analogues modified in position 7 of the benzofuranone ring [54]. Moreover, they are also strong apoptosis inducers that follow the mitochondrial intrinsic pathway. They did not show any appreciable activity on normal human lymphocytes, suggesting a low toxicity profile. It is worth noting that the replacement of bromine with a methyl group or a more bulky substituent such as 4-methylphenyl (compound **5**) did not substantially modify the cytotoxic potency in comparison with **2**, suggesting the existence of a large binding pocket in tubulin. From the point of view of the inhibition of tubulin polymerization *in vitro*, 9′-bromonoscapine and related derivatives did not show potent activity. The most active compound had an IC_{50} of 120 μM, 100 fold weaker than that

observed for CA-4. However, our results indicate, as have those presented by other workers, that noscapine and, in particular, 9′-bromonoscapine may produce subtle effects on microtubule dynamics that could interfere, for example, with the proper attachment of chromosomes to the kinetochore microtubules [55] instead of strongly binding to tubulin as do most well-studied antimitotic drugs. In accord with this idea, it was recently shown [55] that 9′-bromonoscapine did not perturb the morphology of microtubules but rather induced alterations in the centrosome duplication cycle and caused inappropriate centrosome amplification. Our data showed that 9′-substituted noscapine induce accumulation of round cells with condensed DNA indicative of mitotic arrest and in addition, PCM1 alteration disrupted the radial organization of microtubules. We also found that compounds **3–5** induced a substantial increase in the expression of the phosphorylated form of H2AX that is indicative of DNA damage. This could be due to a protracted mitotic arrest that ultimately led to cell death. In conclusion, all these findings indicate that the noscapine derivatives have good therapeutic potential and merit further investigation.

5. Experimental protocol

5.1. Chemistry

5.1.1. Materials and methods—Starting materials were purchased from Sigma–Aldrich and used without further purification. Melting points were determined with a Kofler hot-stage apparatus and are uncorrected. Thin-layer chromatography was performed on pre-coated Merck 5554 Kieselgel 60 F254 foils using CH_2Cl_2:methanol = 8:2 mobile phase. Column chromatography was performed on silica gel 60 (Mesh 230–400 ASTM, grading 0.04–0.063) of the Merck VWR company as stationary phase. As a mobile phase the mixture of CH_2Cl_2:methanol = 9:1 was used for each product.

The spots were visualized with Dragendorff's reagent. ^{1}H NMR spectra were recorded on a Bruker Avance DRX 400 spectrometer, chemical shifts are reported in parts per million (δ) from internal TMS, and coupling constants (*J*) are measured in Hertz. Elemental analyses (C, H, N) were obtained on a Carlo Erba EA1108 analyzer. Optical rotation data were obtained from a Perkin–Elmer 341 polarimeter. CD spectra were recorded on a J-810 spectropolarimeter. The CD spectra were measured in millidegrees and normalized into $\Delta\varepsilon_{max}$ [l mol^{-1} cm^{-1}]/λ [nm] units in spectroscopic grade CH_3CN.

Crystallography data for compound **2** were collected on a Bruker–Nonius MACH3 diffractometer at 293 K, Mo Kα radiation λ = 0.71073 Å, ω motion. All non-hydrogen atoms were refined anisotropically.

5.2. General procedure for the Suzuki coupling of 9′-bromonoscapine (2)

A mixture of 150 mg 9′-bromonoscapine (**2**, M_r 430.1 g/mol; 0.35 mmol), 0.452 mmol of the respective boronic acid, 3 mg palladium(II)acetate (M_r 177.4 g/mol; 0.016 mmol) and 6 mg (2-biphenylyl)-dicyclohexylphosphine (M_r 350.2 g/mol; 0.016 mmol) was dissolved in 6.35 mL THF/methanol (4:1). To the stirred solution, 300 µl K_3PO_4 solution (2 M) was added at room temperature. The temperature was increased to 80 °C, and the reaction mixture was refluxed for 2–5 h. Every hour the progress of the reactionwas followed by

TLC. The reaction was stopped when there was no further progress, and the mixture was evaporated under reduced pressure. Afterward, the solid mixture was separated using column chromatography. The product was then analyzed.

5.2.1. 9′-Methylnoscapine (3)—Amorphous yellow solid; m.p.: 147–149 °C; ^{1}H NMR ($CDCl_3$) δ = 6.98 (1H, d, H5, $J_{4–5}$ = 7.0); 6.13 (1H, d, H4, $J_{4–5}$ = 7.0); 5.93 (2H, s, 2H2′); 5.56 (1H, d, H3, $J_{5′–3}$ = 4.5); 4.40 (1H, d, H5′, $J_{5′–3}$ = 4.5); 4.09 (3H, s, OCH_3); 3.96 (3H, s, OCH_3); 3.87 (3H, s, OCH_3); 2.76–2.33 (7H, m, NCH_3, H7′α, H7′β, H8′a, H8′β); 2.06 (3H, s, C9′-CH_3); ^{13}C NMR ($CDCl_3$) δ = 168.4 (C═O); 153.1 (C6); 151.7 (C1′a); 150.1 (C4′a); 147.4 (C7); 140.1 (C3a); 135.9 (C3′a); 131.0 (C8′a); 121.7 (C4′a); 118.3 (C7a); 118.0 (C5); 116.4 (C4); 116.3 (C9′); 100.7 (C2′); 82.1 (C3); 69.7 (C5′); 61.2 (OCH_3); 59.7 (OCH_3); 57.1 (OCH_3); 49.4 (C7′); 46.0 (NCH_3); 24.1 (C8′); 11.2 (C9′-$\underline{C}H_3$); IR (KBr pellet, cm^{-1}): 3448; 2963; 1762; 1262; 1092; 1023; calculated for $C_{23}H_{25}NO_7$: C, 64.63; H, 5.90; N, 3.28; found: C, 64.69; H, 5.99; N, 3.34.

5.2.2. 9′-Phenylnoscapine (4)—Light yellow crystals; m.p.: 78–80 °C; ^{1}H NMR ($CDCl_3$) δ = 7.45–7.21 (5H, m, ar); 7.10 (1H, d, H5, $J_{4–5}$ = 6.7); 6.15 (1H, d, H4, $J_{4–5}$ = 6.7); 5.98 (2H, d, 2H2′, J = 18.8); 5.58 (1H, d, H3, $J_{5′–3}$ = 4.9); 4.52 (1H, d, H5′, $J_{5′–3}$ = 4.9); 4.13 (3H, s, OCH_3); 4.12 (3H, s, OCH_3); 3.92 (3H, s, OCH_3); 2.58 (3H, s, NCH_3); 2.38–2.18 (4H, m, H7′α, H7′β, H8′a, H8′β); ^{13}C NMR ($CDCl_3$) δ = 173.3 (C═O); 157.6 (C6); 154.0 (C1′a); 148.2 (C4′); 148.0 (C7); 142.3 (ar); 137.9 (C3a); 135.8 (C3′a); 132.8 (C8′a); 130.2 (2 ar); 129.5 (2 ar); 127.8 (ar); 118.2 (C4′a); 117.6 (C7a); 115.9 (C5); 112.1 (C4); 108.4 (C9′); 101.1 (C2′); 82.2 (C3); 68.2 (C5′); 61.4 (OCH_3); 59.8 (OCH_3); 57.2 (OCH_3); 51.1 (C7′); 47.0 (NCH_3); 24.2 (C8′); IR (KBr pellet, cm^{-1}): 3443; 2963; 1762; 1261; 1091; 1035; calculated for $C_{28}H_{27}NO_7$: C, 68.70; H, 5.56; N, 2.86; found: C, 68.69; H, 5.61; N, 2.91.

5.2.3. 9′-(4-Methylphenyl)-noscapine (5)—Yellow amorphous solid; ^{1}H NMR ($CDCl_3$) δ = 8.14 (2H, d, ar); 7.35–7.16 (2H, m, ar); 7.04 (1H, d, H5, $J_{4–5}$ = 7.1); 6.17 (1H, d, H4, $J_{4–5}$ = 7.1); 5.95 (2H, d, 2H2′, J = 15.2); 5.61 (1H, d, H3, $J_{5′–3}$ = 4.5); 4.47 (1H, d, H5′, $J_{5′–3}$ = 4.5); 4.14 (3H, s, OCH_3); 4.11 (3H, s, OCH_3); 3.93 (3H, s, OCH_3); 2.59 (3H, s, NCH_3); 2.41 (3H, s, C4″-CH_3); 2.34–2.07 (4H, m, H7′α, H7′β, H8′a, H8′β); ^{13}C NMR ($CDCl_3$) δ = 167.4 (C═O); 152.3 (C6); 151.7 (C1′a); 151.1 (C4′); 148.3 (C7); 141.9 (ar); 139.9 (C3a); 138.8 (ar); 135.6 (C3′a); 131.8 (C8′a); 129.8 (2 ar); 129.0 (2 ar); 117.9 (C4′a); 117.7 (C7a); 115.0 (C5); 111.8 (C4); 109.8 (C9′); 100.8 (C2′); 82.0 (C3); 69.9 (C5′); 61.1 (OCH_3); 59.6 (OCH_3); 56.9 (OCH_3); 51.0 (C7′); 46.8 (NCH_3); 25.1 (C8′); 21.7 (C4″-$\underline{C}H_3$); IR (KBr pellet, cm^{-1}): 3448; 2962; 1760; 1262; 1084; 1034; calculated for $C_{29}H_{29}NO_7$: C, 69.17; H, 5.80; N, 2.78; found: C, 69.30; H, 5.91; N, 2.71.

5.2.4. 9′-(2-Methoxyphenyl)-noscapine (6)—Pale brown amorphous product; m.p.: 192–195 °C; ^{1}H NMR ($CDCl_3$) δ = 7.34–6.89 (5H, m, ar, H5); 6.26 (1H, d, H4, $J_{4–5}$ = 7.1); 5.85 (2H, s, 2H2′); 5.58 (1H, d, H3, $J_{5′–3}$ = 5.0); 4.41 (1H, d, H5′, $J_{5′–3}$ = 5.0); 4.04 (6H, s, 2 OCH_3); 3.81 (3H, s, OCH_3); 3.75 (3H, s, OCH_3); 2.49 (3H, s, NCH_3); 2.21–1.98 (4H, m, H7′α, H7′β, H8′a, H8′β); ^{13}C NMR ($CDCl_3$) δ = 168.7 (C═O); 157.9 (ar); 153.1 (C6); 151.8 (C1′a); 148.3 (C4′); 147.9 (C7); 145.0 (ar); 139.0 (C3a); 134.3 (C3′a); 132.4 (C8′a);

130.8 (ar); 128.4 (ar); 119.6 (2 ar); 117.5 (C4′a); 117.3 (C7a); 116.8 (C5); 111.6 (C4); 110.0 (C9′); 99.8 (C2′); 81.4 (C3); 66.4 (C5′); 60.2 (OCH_3); 58.5 (OCH_3); 55.9 (OCH_3); 54.5 (OCH_3); 50.0 (C7′); 45.9 (NCH_3); 25.0 (C8′); IR (KBr pellet, cm^{-1}): 3447; 2962; 1753; 1261; 1114; 1083; 1036; calculated for $C_{29}H_{29}NO_8$: C, 67.04; H, 5.63; N, 2.70; found: C, 67.12; H, 5.58; N, 2.54.

5.2.5. 9′-(3-Methoxyphenyl)-noscapine (7)—Off-white amorphous product; m.p.: 155–157 °C; ^{1}H NMR ($CDCl_3$) δ = 7.47–6.95 (5H, m, ar, H5); 6.24 (1H, d, H4, $J_{4–5}$ = 8.0); 5.83 (2H, s, 2H2′); 5.58 (1H, d, H3, $J_{5′–3}$ = 4.8); 4.44 (1H, d, H5′, $J_{5′–3}$ = 4.8); 4.07 (6H, s, 2 OCH_3); 3.81 (3H, s, OCH_3); 3.71 (3H, s, OCH_3); 2.44 (3H, s, NCH_3); 2.29–2.00 (4H, m, H7′α, H7′β, H8′a, H8′β); ^{13}C NMR ($CDCl_3$) δ = 166.4 (C═O); 161.8 (ar); 152.8 (C6); 151.8 (C1′a); 148.4 (C4′); 147.3 (C7); 144.4 (ar); 138.6 (C3a); 134.4 (C3′a); 134.1 (C8′a); 131.0 (ar); 128.4 (ar); 120.6 (2 ar); 118.0 (C4′a); 117.6 (C7a); 117.0 (C5); 112.4 (C4); 110.9 (C9′); 99.5 (C2′); 81.8 (C3); 66.6 (C5′); 61.0 (OCH_3); 59.4 (OCH_3); 56.7 (OCH_3); 55.5 (OCH_3); 50.9 (C7′); 44.4 (NCH_3); 23.0 (C8′); IR (KBr pellet, cm^{-1}): 3441; 2955; 1750; 1270; 1111; 1080; 1036; calculated for $C_{29}H_{29}NO_8$: C, 67.04; H, 5.63; N, 2.70; found: C, 67.00; H, 5.69; N, 2.81.

5.2.6. 9′-(4-Methoxyphenyl)-noscapine (8)—Off-white amorphous product; m.p.: 167–169 °C; ^{1}H NMR ($CDCl_3$) δ = 7.62–7.55 (2H, m, ar); 7.12–7.05 (3H, m, ar, H5), 6.28 (1H, d, H4, $J_{4–5}$ =7.0); 5.81 (2H, s, 2H2′); 5.54 (1H, d, H3, $J_{5′–3}$ =5.0); 4.47 (1H, d, H5′, $J_{5′–3}$ = 5.0); 4.00 (6H, s, 2 OCH_3); 3.81 (3H, s, OCH_3); 3.78 (3H, s, OCH_3); 2.44 (3H, s, NCH_3); 2.30–1.94 (4H, m, H7′α, H7′β, H8′a, H8′β); ^{13}C NMR ($CDCl_3$) δ= 168.4 (C═O); 159.1 (ar); 153.1 (C6); 152.0 (C1′a); 148.7 (C4′); 148.0 (C7); 145.4 (ar); 139.0 (C3a); 134.3 (C3′a); 132.4 (C8′a); 130.8 (2 ar); 128.4 (ar); 119.6 (ar); 117.5 (C4′a); 117.3 (C7a); 116.8 (C5); 111.6 (C4); 110.0 (C9′); 99.8 (C2′); 81.4 (C3); 66.4 (C5′); 60.2 (OCH_3); 58.5 (OCH_3); 55.9 (OCH_3); 54.5 (OCH_3); 50.0 (C7′); 45.4 (NCH_3); 23.8 (C8′); IR (KBr pellet, cm−1): 3441; 2960; 1761; 1255; 1114; 1087; 1039; calculated for $C_{29}H_{29}NO_8$: C, 67.04; H, 5.63; N, 2.70; found: C, 66.95; H, 5.54; N, 2.84.

5.2.7. 9′-(2-Naphthyl)-noscapine (9)—Pale brown amorphous product; m.p.: 101–103 °C; ^{1}H NMR ($CDCl_3$) δ = 8.03–7.53 (7H, m, ar); 7.01 (1H, d, H5, $J_{4–5}$ = 7.0); 6.21 (1H, d, H4, $J_{4–5}$ =7.0); 5.87 (2H, s, 2H2′); 5.53 (1H, d, H3, $J_{5′–3}$ = 4.7); 4.33 (1H, d, H5′, $J_{5′–3}$ = 4.7); 4.01 (6H, s, 2 OCH_3); 3.84 (3H, s, OCH_3); 2.47 (3H, s, NCH_3); 2.24–1.99 (4H, m, H7′α, H7′β, H8′a, H8′β); ^{13}C NMR ($CDCl_3$) δ= 168.7 (C═O); 152.8 (C6); 151.7 (C1′a); 148.1 (C4′); 148.0 (C7); 138.8 (C3a); 137.4 (ar), 136.9 (ar), 136.5 (ar) 135.7 (2 ar), 134.2 (C3′a); 131.9 (C8′a); 130.2 (2 ar); 128.7 (2 ar); 119.9 (ar); 118.0 (C4′a); 117.2 (C7a); 116.5 (C5); 111.4 (C4); 109.8 (C9′); 99.5 (C2′); 81.5 (C3); 66.9 (C5′); 60.1 (OCH_3); 59.1 (OCH_3); 56.2 (OCH_3); 55.0 (OCH_3); 50.4 (C7′); 44.4 (NCH_3); 23.2 (C8′); IR (KBr pellet, cm^{-1}): 3448; 2959; 1758; 1252; 1110; 1087; 1035; calculated for $C_{32}H_{29}NO_7$: C, 71.23; H, 5.42; N, 2.60; found: C, 71.12; H, 5.53; N, 2.54.

5.3. Biology

5.3.1. Antiproliferative assays—Human T-cell (Jurkat) and B-cell leukemia cell lines (SEM and RS4; 11) were grown in RPMI-1640 medium (Gibco, Milano, Italy). Human

breast adenocarcinoma (MCF7), non-small cell lung carcinoma (A549), cervix carcinoma (HeLa), ovarian carcinoma (IGROV- 1) and colon adenocarcinoma (HT-29) cells were grown in DMEM medium (Gibco, Milano, Italy), all supplemented with 115 units/mL of penicillin G (Gibco, Milano, Italy), 115 μg/mL of streptomycin (Invitrogen, Milano, Italy) and 10% fetal bovine serum (Invitrogen, Milano, Italy). Stock solutions (10 mM) of the different compounds were prepared by dissolving them in dimethyl sulfoxide (DMSO). Individual wells of a 96-well tissue culture microtiter plate were inoculated with 100 μL of complete medium containing $8 \times 10_3$ cells. The plates were incubated at 37 °C in a humidified 5% CO_2 incubator for 18 h prior to compound addition. After medium removal, 100 μL of fresh medium containing the test compound at different concentrations was added to each well, and the plates were incubated at 37 °C for 72 h. Cell viability was assayed by the (3-(4,5-dimethylthiazol-2-yl)-2,5-diphenyl tetrazolium bromide) test as previously described [56].

5.3.2. Effects on tubulin polymerization and on colchicine binding to tubulin— Tubulin assembly was measured by turbidimetry at 350 nm in Gilford model 250 spectrophotometers equipped with electronic temperature controllers. Reaction mixtures containing purified bovine brain tubulin [15] at 10 μM(1.0 mg/mL), 0.8Mmonosodium glutamate (pH 6.6 with HCl in 2 M stock solution), 4% (v/v) DMSO, and varying compound concentrations were preincubated 15 min at 30 °C in 0.24 mL. The mixtures were then chilled on ice, and 10 μL of 10 mM GTP was added (final concentration, 0.4 mM). All concentrations refer to the final volume of 0.25 mL. The samples were transferred to 0 °C cuvettes in the spectrophotometers, and the temperature was jumped to 30 °C over about 1 min. Either the maximum reaction rate (occurring at varying times) or the extent of assembly after 20 min was measured. The colchicine binding assay was measured as described in detail previously [57]. Reaction mixtures (0.1 mL) contained 1.0 μM tubulin, 5.0 μM [^{3}H]colchicine (from Perkin–Elmer), the potential inhibitor at 5 or 500 μM, 5% DMSO, and the tubulin stabilizing components described previously [58,59]. Incubation was for 10 min at 37 °C, and the bound colchicine was trapped through the tubulin on a stack of two Whatman DEAE-cellulose filters (from GE Healthcare Life Sciences) and quantitated by liquid scintillation counting.

5.3.3. Immunofluorescence analysis—Cells were fixed in cold 4% formaldehyde for 15 min, rinsed and stored prior to analysis. Primary antibody staining was performed for β-tubulin (mouse, monoclonal 1:1000, Sigma–Aldrich, Milano, Italy). After incubation, cells were washed and incubated with an Alexa conjugated secondary antibody (1:2000, Life Technologies, Monza, Italy). Cells were counterstained with 4′,6-diamidin-2-fenilindole (DAPI) (1:10,000, Sigma–Aldrich, Milano, Italy). Images were obtained on a video-confocal microscope (Vico, Eclipse Ti80, Nikon), equipped with a digital camera.

5.3.4. Evaluation of mitotic index—The Burkitt lymphoma CA46 cells were grown in RPMI 1640 medium supplemented with 17% fetal bovine serum and 2 mM L-glutamine at 37 °C 5% CO_2 atmosphere. The mitotic index in the Burkitt cell cultures was determined at 16 h, the time that produces a near-maximal value after treatment with antitubulin drugs. About 4.5 ml of cell culture medium was centrifuged at 1000 rpm for 1 min. The pelleted

cells were resuspended in 5 ml of phosphate-buffered saline at room temperature, and the cells were harvested by centrifuging the suspension as before. The cell pellet was suspended in 0.5 ml of half-strength phosphate-buffered saline, and the cells were allowed to swell for 10 min. The cells were then fixed by adding 6 ml of 0.5% acetic acid-1.5% ethanol. After 30 min, the cells were harvested by centrifuging as before. The cells were resuspended in 25% acetic acid/75% ethanol, and a droplet of the cell suspension was spread on the slide. The slide was air-dried and stained with Giemsa. The slide was examined under a light microscope, with mitotic cells defined as those with condensed chromosomes and no nuclear membrane. At least 200 cells were counted for each condition examined.

5.3.5. Flow cytometric analysis of cell cycle distribution—For flow cytometric analysis of DNA content, 5×10^5 HeLa or Jurkat cells were treated with different concentrations of the test compounds for 24 or 48 h. After the incubation period, the cells were collected, centrifuged and fixed with ice-cold ethanol (70%). The cells were then treated with lysis buffer containing RNAse A and 0.1% Triton X-100 and stained with propidium iodide (PI). Samples were analyzed on a Cytomic FC500 flow cytometer (Beckman Coulter). DNA histograms were analyzed using Multi- Cycle® for Windows (Phoenix Flow Systems).

5.3.6. Annexin-V assay—Surface exposure of phosphatidyl serine (PS) on apoptotic cells was measured by flow cytometry with a Coulter Cytomics FC500 (Beckman Coulter) by adding annexin-V-FITC to cells according to the manufacturer's instructions (Annexin-V Fluos, Roche Diagnostic). Simultaneously, the cells were stained with PI. Excitation was set at 488 nm, and the emission filters were at 525 and 585 nm, respectively, for FTIC and PI.

5.3.7. Assessment of mitochondrial changes—The mitochondrial membrane potential was measured with the lipophilic cationic dye 5,5′,6,6′-tetrachlo-1,1′,3,3′-tetraethylbenzimidazolcarbocyanine (JC-1) (Molecular Probes), as described [56]. The production of reactive oxygen species (ROS) was measured by flow cytometry using 2,7-dichlorodihydrofluorescein diacetate (H_2DCFDA) (Molecular Probes), as previously described [54].

5.3.8. Western blot analysis—HeLa cells were incubated in the presence of test compounds and, after different times, were collected, centrifuged and washed two times with ice cold phosphate-buffered saline (PBS). The pellet was then resuspended in lysis buffer. After the cells were lysed on ice for 30 min, lysates were centrifuged at 15,000 × *g* at 4 °C for 10 min. The protein concentration in the supernatants was determined using the BCA protein assay reagents (Pierce, Italy). Equal amounts of protein (20 μg) were resolved using sodium dodecyl sulfate polyacrylamide gel electrophoresis (SDS-PAGE) (7.5–15% acrylamide gels) and transferred to PVDF Hybond-p membrane (GE Healthcare). Membranes were blocked with I-block (Tropix), the membrane being gently rotated overnight at 4 °C. Membranes were then incubated with primary antibodies against Bcl-2, Bax, cleaved poly(ADP-ribose) polymerase (PARP), cleaved caspase-9, pcdc2^{Tyr15}, cdc25c (Cell Signaling), caspase-3 (Alexis), cyclin B (Upstate) or β-actin (Sigma–Aldrich) for 2 h at room temperature. Membranes were next incubated with peroxidase-labeled secondary

antibodies for 60 min. All membranes were visualized using ECL Advance (GE Healthcare) and exposed to Hyperfilm MP (GE Healthcare). To ensure equal protein loading, each membrane was stripped and reprobed with anti-β-actin antibody.

Acknowledgments

This research was supported by the European Union and the State of Hungary (OTKA Grant No. 101372), co-financed by the European Social Fund in the framework of TÁMOP 4.2.4. A/2-11-1-2012-0001 'National Excellence Program'.

References

1. Hadfield JA, Ducki S, Hirst N, McGown AT. Tubulin and microtubules as targets for anticancer drugs. Prog. Cell Cycle Res. 2003; 5:309–325. [PubMed: 14593726]
2. Jordan MA, Wilson L. Microtubules as a target for anticancer drugs. Nat. Rev. Cancer. 2004; 4:253–265. [PubMed: 15057285]
3. Dumontet C, Jordan MA. Microtubule-binding agents: a dynamic field of cancer therapeutics. Nat. Rev. Drug Discov. 2010; 9:790–803. [PubMed: 20885410]
4. Ye K, Ke Y, Keshava N, Shanks J, Kapp JA, Tekmal RR, Petros J, Joshi HC. Opium alkaloid noscapine is an antitumor agent that arrests metaphase and induces apoptosis in dividing cells. Proc. Natl. Acad. Sci. U. S. A. 1998; 95:1601–1606. [PubMed: 9465062]
5. Mahmoudian M, Rahimi-Moghaddam P. The Anti-cancer activity of noscapine: a review. Recent Pat. Anticancer Drug Discov. 2009; 4:92–97. [PubMed: 19149691]
6. Joshi, HC.; Ye, K.; Kapp, J.; Liu, F. Noscapine and Noscapine Derivatives Useful as Anticancer Agents. U.S. Patent. 6,376,516. 04.2002. 2002.
7. Zhou J, Gupta K, Aggarwal S, Aneja R, Chandra R, Panda D, Joshi HC. Brominated derivatives of noscapine are potent microtubule-interfering agents that perturb mitosis and inhibit cell proliferation. Mol. Pharmacol. 2003; 63:799–807. [PubMed: 12644580]
8. Aneja R, Vangapandu SN, Lopus M, Chandra R, Panda D, Joshi HC. Development of a novel nitro-derivative of noscapine for the potential treatment of drug-resistant ovarian cancer and T-cell lymphoma. Mol. Pharmacol. 2006; 69:1801–1809. [PubMed: 16517755]
9. Manchukonda NK, Sridhar B, Naik PK, Joshi HC, Kantevari S. Copper(I) mediated facile synthesis of potent tubulin polymerization inhibitor, 9-aminoalpha- noscapine from natural α-noscapine. Bioorg. Med. Chem. Lett. 2012; 22:2983–2987. [PubMed: 22425569]
10. Naik PK, Chatterji BP, Vangapandu SN, Aneja R, Chandra R, Kanteveri S, Joshi HC. Rational design, synthesis and biological evaluations of aminonoscapine: a high affinity tubulin-binding noscapinoid. J. Comput. Aided Mol. Des. 2011; 25:443–454. [PubMed: 21544622]
11. Bognár R, Gaál G, Kerekes P, Szabó S. On the accompanying alkaloids of morphine. 1. Isolation of codeine, thebaine and narcotine (in German). Pharmazie. 1967; 22:452–456. [PubMed: 5601618]
12. Baradarani MM, Prager RH. The specific epimerization of phthalideisoquinoline alkaloids. Tetrahedron Lett. 1999; 40:7403–7406.
13. Miyaura N, Suzuki A. Palladium-catalyzed cross-coupling reactions of organoboron compounds. Chem. Rev. 1995; 95:2457–2483.
14. Berényi S, Sipos A, Szabó I, Kálai T. Novel route to 2-arylapomorphines. Synth. Commun. 2007; 37:467–471.
15. Sipos A, Debreceni S, Szabó R, Gyulai Z, Berényi S. Synthesis of 3-alkyl and arylapomorphines. Synth. Commun. 2007; 37:2549–2558.
16. Sipos A, Berényi S, Kiss B, Schmidt É, Greiner I. Synthesis and neurophar-macological evaluation of 2-aryl- and alkylapomorphines. Bioorg. Med. Chem. 2008; 16:3773–3779. [PubMed: 18289859]
17. Martin R, Buchwald SL. Palladium-catalyzed Suzuki–Miyaura cross-coupling reactions employing dialkylbiaryl phosphine ligands. Acc. Chem. Res. 2008; 41:1461–1473. [PubMed: 18620434]

18. Snatzke G, Wollenberg G, Hrbek J Jr, Santavy F, Blaha K, Klyne W, Swan JR. The optical rotatory dispersion and circular dichroism of the phthalideisoquinoline alkaloids and of their α-hydroxybenzyltetrahydroisoquinoline derivatives. Tetrahedron. 1969; 25:5059–5075.
19. von Langermann J, Lorenz H, Boehm O, Fleming A, Bernsdorf A, Köckerling M, Schinzer D, Seidel-Morgenstern A. (3*R**,5′*S**)-6,7-Dimethoxy-3-(4′-methoxy-6′-methyl-5′,6′,7′,8′-tetrahydro-1,3-dioxolo[4,5-*g*]isoquinolin-5′-yl)isobenzofuran-1(3*H*)-one (racemic-noscapine). Acta Cryst. 2010; E66:o570–o572.
20. Seetharaman J, Rajan SS. Crystal and molecular-structure of noscapine. Zeit Krist. 1995; 210:111–113.
21. Naik PK, Santoshi S, Joshi HC. Noscapinoids with anti-cancer activity against human acute lymphoblastic leukemia cells (CEM): a three dimensional chemical space pharmacophore modeling and electronic feature analysis. J. Mol. Model. 2012; 18:307–318. [PubMed: 21523542]
22. Hamel E. Evaluation of antimitotic agents by quantitative comparisons of their effects on the polymerization of purified tubulin. Cell Biochem. Biophys. 2003; 38:1–22. [PubMed: 12663938]
23. Pinney KG, Bounds AD, Dingeman KM, Mocharla VP, Pettit GR, Bai R, Hamel E. A new anti-tubulin agent containing the benzo[*b*]thiophene ring system. Bioorg. Med. Chem. Lett. 1999; 9:1081–1086. [PubMed: 10328289]
24. Raffa D, Maggio B, Plescia F, Cascioferro S, Plescia S, Raimondi MV, Daidone G, Tolomeo M, Grimaudo S, Di Cristina A, Pipitone RM, Bai R, Hamel E. Synthesis, antiproliferative activity, and mechanism of action of a series of 2-{[2*E*]-3-phenylprop-2-enoylamino}benzamides. Eur. J. Med. Chem. 2011; 46:2786–2796. [PubMed: 21530013]
25. Hamel E, Blokhin AV, Nagle DG, Yoo HD, Gerwick WH. Limitations in the use of tubulin polymerization assays as a screen for the identification of new antimitotic agents: the potent marine natural product curacin A as an example. Drug Dev. Res. 1995; 34:110–120.
26. Edler MC, Yang G, Jung MK, Bai R, Bornmann WG, Hamel E. Demonstration of microtubule-like structures formed with (−)-rhazinilam from purified tubulin outside of cells and a simple tubulin-based assay for evaluation of analog activity. Arch. Biochem. Biophys. 2009; 407:98–104. [PubMed: 19497297]
27. Lin CM, Kang GJ, Roach MC, Jiang JB, Hesson DP, Ludueña RF, Hamel E. Investigation of the mechanism of the interaction of tubulin with derivatives of 2-styrylquinazolin-4(3*H*)-one. Mol. Pharmacol. 1991; 40:827–832. [PubMed: 1944246]
28. Kang GJ, Getahun Z, Muzaffar A, Brossi A, Hamel E. *N*-acetylcolchinol *O*-methyl ether and thiocolchicine, potent analogs of colchicine modified in the C ring: evaluation of the mechanistic basis for their enhanced biological properties. J. Biol. Chem. 1990; 265:10255–10259. [PubMed: 2191947]
29. Naik PK, Santoshi S, Rai A, Joshi HC. Molecular modeling and competition binding study of Br-noscapine and colchicine provide insight into noscapinoid-tubulin binding site. J. Mol. Graph. Model. 2011; 29:947–955. [PubMed: 21530342]
30. Bhattacharyya B, Wolff J. Promotion of fluorescence upon binding of colchicine to tubulin. Proc. Natl. Acad. Sci. U. S. A. 1974; 71:2627–2631. [PubMed: 4527949]
31. Kubo A, Tsukita S. Non-membranous granular organelle consisting of PCM-1: subcellular distribution and cell-cycle-dependent assembly/disassembly. J. Cell Sci. 2003; 116:919–928. [PubMed: 12571289]
32. Balczon R, Bao L, Zimmer WE. PCM-1, A 228-kD centrosome autoantigen with a distinct cell cycle distribution. J. Cell Biol. 1994; 124:783–793. [PubMed: 8120099]
33. Didier C, Merdes A, Gairin JE, Jabrane-Ferrat N. Inhibition of proteasome activity impairs centrosome-dependent microtubule nucleation and organization. Mol. Biol. Cell. 2008; 19:1220–1229. [PubMed: 18094058]
34. Clarke PR, Allan LA. Cell-cycle control in the face of damage – a matter of life or death. Trends Cell Biol. 2009; 19:89–98. [PubMed: 19168356]
35. Kiyokawa H, Ray D. In vivo roles of cdc25 phosphatases: biological insight into the anti-cancer therapeutic targets. Anticancer Agents Med. Chem. 2008; 8:832–836. [PubMed: 19075565]
36. Donzelli M, Draetta GF. Regulating mammalian checkpoints through cdc25 inactivation. EMBO Rep. 2003; 4:671–677. [PubMed: 12835754]

37. Walter AO, Seghezzi W, Korver W, Sheung J, Lees E. The mitotic serine/threonine kinase aurora2/AIK is regulated by phosphorylation and degradation. Oncogene. 2000; 19:4906–4916. [PubMed: 11039908]
38. Quignon F, Rozier L, Lachages AM, Bieth A, Simili M, Debatisse M. Sustained mitotic block elicit DNA breaks: one step alteration of ploidy and chromosome integrity in mammalian cells. Oncogene. 2007; 26:165–172. [PubMed: 16832348]
39. Ganem NJ, Pellman D. Linking abnormal mitosis to the acquisition of DNA damage. J. Cell Biol. 2012; 199:871–881. [PubMed: 23229895]
40. Vermes I, Haanen C, Steffens-Nakken H, Reutelingsperger C. A novel assay for apoptosis. Flow cytometric detection of phosphatidylserine expression on early apoptotic cells using fluorescein labelled annexin V. J. Immunol. Method. 1995; 184:39–51.
41. Green DR, Kroemer G. The pathophysiology of mitochondrial cell death. Science. 2005; 305:626–629. [PubMed: 15286356]
42. Ly JD, Grubb DR, Lawen A. The mitochondrial membrane potential ($\Delta\psi_m$) in apoptosis: an update. Apoptosis. 2003; 3:115–128. [PubMed: 12766472]
43. Cai J, Jones DP. Superoxide in apoptosis. Mitochondrial generation triggered by cytochrome *c* loss. J. Biol. Chem. 1998; 273:11401–11404. [PubMed: 9565547]
44. Mollinedo F, Gajate C. Microtubules, microtubule-interfering agents and apoptosis. Apoptosis. 2003; 8:413–450. [PubMed: 12975575]
45. Chiang NJ, Lin CI, Liou JP, Kuo CC, Chang CY, Chen LT, Chang JY. A novel synthetic microtubule inhibitor, MPT0B214 exhibits antitumor activity in human tumor cells through mitochondria-dependent intrinsic pathway. Plos One. 2013; 8(3):e58953. [PubMed: 23554962]
46. Romagnoli R, Baraldi PG, Lopez-Cara C, Kimatrai Salvador M, Preti D, Aghazadeh Tabrizi M, Bassetto M, Brancale A, Hamel E, Castagliuolo I, Bortolozzi R, Basso G, Viola G. Synthesis and biological evaluation of 2- alkoxycarbonyl-3-anilino benzo[*b*]thiophenes and thieno[2,3-*b*]pyridines as new potent anticancer agents. J. Med. Chem. 2013; 56:2606–2618. [PubMed: 23445496]
47. Denault JB, Salvesen GS. Caspases: keys in the ignition of cell death. Chem. Rev. 2002; 102:4489–4499. [PubMed: 12475198]
48. Porter AG, Janicke RU. Emerging role of caspase-3 in apoptosis. Cell Death Differ. 1999; 6:99–104. [PubMed: 10200555]
49. Aneja R, Zhou J, Vangapandu SN, Zhou B, Chandra R, Joshi HC. Drugresistant T-lymphoid tumors undergo apoptosis selectively in response to an antimicrotubule agent, EM011. Blood. 2006; 107:2486–2492. [PubMed: 16282340]
50. Aneja R, Miyagi T, Karna P, Ezell T, Shukla D, Vij Gupta M, Yates C, Chinni SR, Zhau H, Chung LW, Joshi HC. A novel microtubule-modulating agent induces mitochondrially driven caspase-dependent apoptosis via mitotic checkpoint activation in human prostate cancer cells. Eur. J. Cancer. 2010; 46:1668–1678. [PubMed: 20303260]
51. Wertz IE, Kusam S, Lam C, Okamoto T, Sandoval W, Anderson DJ, Helgason E, Ernst JA, Eby M, Liu J, Belmont LD, Kaminker JS, O'Rourke KM, Pujara K, Kohli PB, Johnson AR, Chiu ML, Lill JR, Jackson PK, Fairbrother WJ, Seshagiri S, Ludlam MJ, Leong KG, Dueber EC, Maecker H, Huang DC, Dixit VM. Sensitivity to antitubulin chemotherapeutics is regulated by MCL1 and FBW7. Nature. 2011; 471:110–114. [PubMed: 21368834]
52. Matson DR, Stukenberg PT. Spindle poisons and cell fate: a tale of two pathways. Mol. Interv. 2011; 11:141. [PubMed: 21540474]
53. DeBono AJ, Xie JH, Ventura S, Pouton CW, Capuano B, Scammells PJ. Synthesis and biological evaluation of N-substituted noscapine analogues. ChemMedChem. 2012; 7:2122–2133. [PubMed: 23055449]
54. Mishra RC, Karna P, Gundala SR, Pannu V, Stanton RA, Gupta KK, Robindon M, Lopus M, Wilson L, Henary M, Aneja R. Biochem. Pharmacol. 2011; 82:110–121. [PubMed: 21501599]
55. Karna P, Rida PC, Pannu V, Gupta KK, Dalton WB, Joshi H, Yang VW, Zhou J, Aneja R. A novel microtubule-modulating noscapinoid triggers apoptosis by inducing spindle multipolarity via centrosome amplification and declustering. Cell Death Differ. 2011; 18:632–644. [PubMed: 21052096]

56. Viola G, Vedaldi D, Dall'Acqua F, Fortunato E, Basso G, Bianchi N, Zuccato C, Borgatti M, Lampronti I, Gambari R. Induction of γ-globin mRNA, erythroid differentiation and apoptosis in UVA-irradiated human erythroid cells in the presence of furocoumarine derivatives. Biochem. Pharm. 2008; 75:810–825. [PubMed: 18022602]

57. Hamel E, Lin CM. Separation of active tubulin and microtubule-associated proteins by ultracentrifugation and isolation of a component causing the formation of microtubule bundles. Biochemistry. 1984; 23:4173–4184. [PubMed: 6487596]

58. Verdier-Pinard P, Lai JY, Yoo HD, Yu J, Márquez B, Nagle DG, Nambu M, White JD, Falck JR, Gerwick WH, Day BW, Hamel E. Structure-activity analysis of the interaction of curacin A, the potent colchicine site antimitotic agent, with tubulin and effects of analogs on the growth of MCF-7 breast cancer cells. Mol. Pharmacol. 1998; 53:62–76. [PubMed: 9443933]

59. Hamel E, Lin CM. Stabilization of the colchicine-binding activity of tubulin by organic acids. Biochim. Biophys. Acta. 1981; 675:226–231. [PubMed: 6115675]

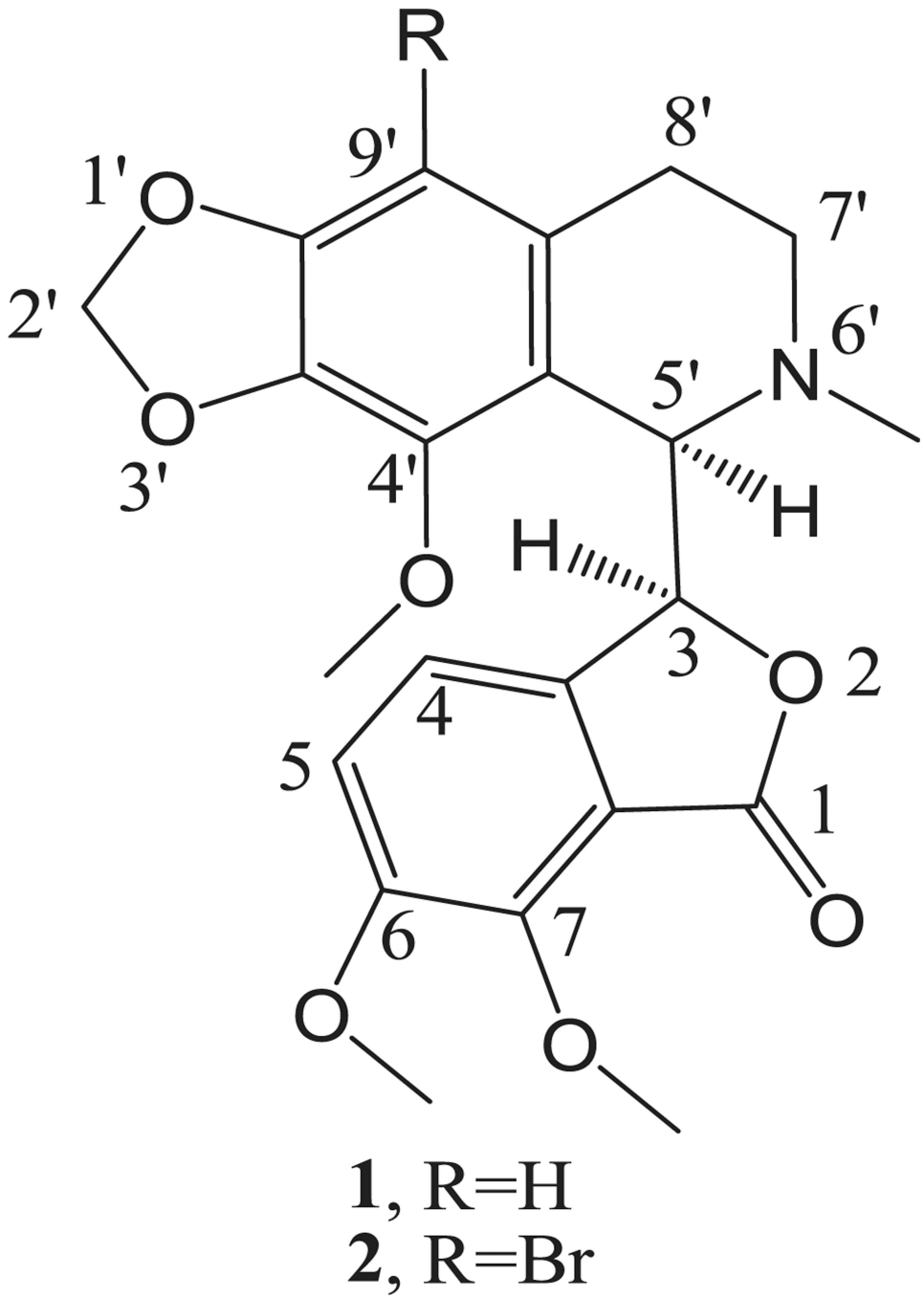

Fig. 1.
The structure of natural noscapine (**1**) and its 9′-bromo derivative **2**.

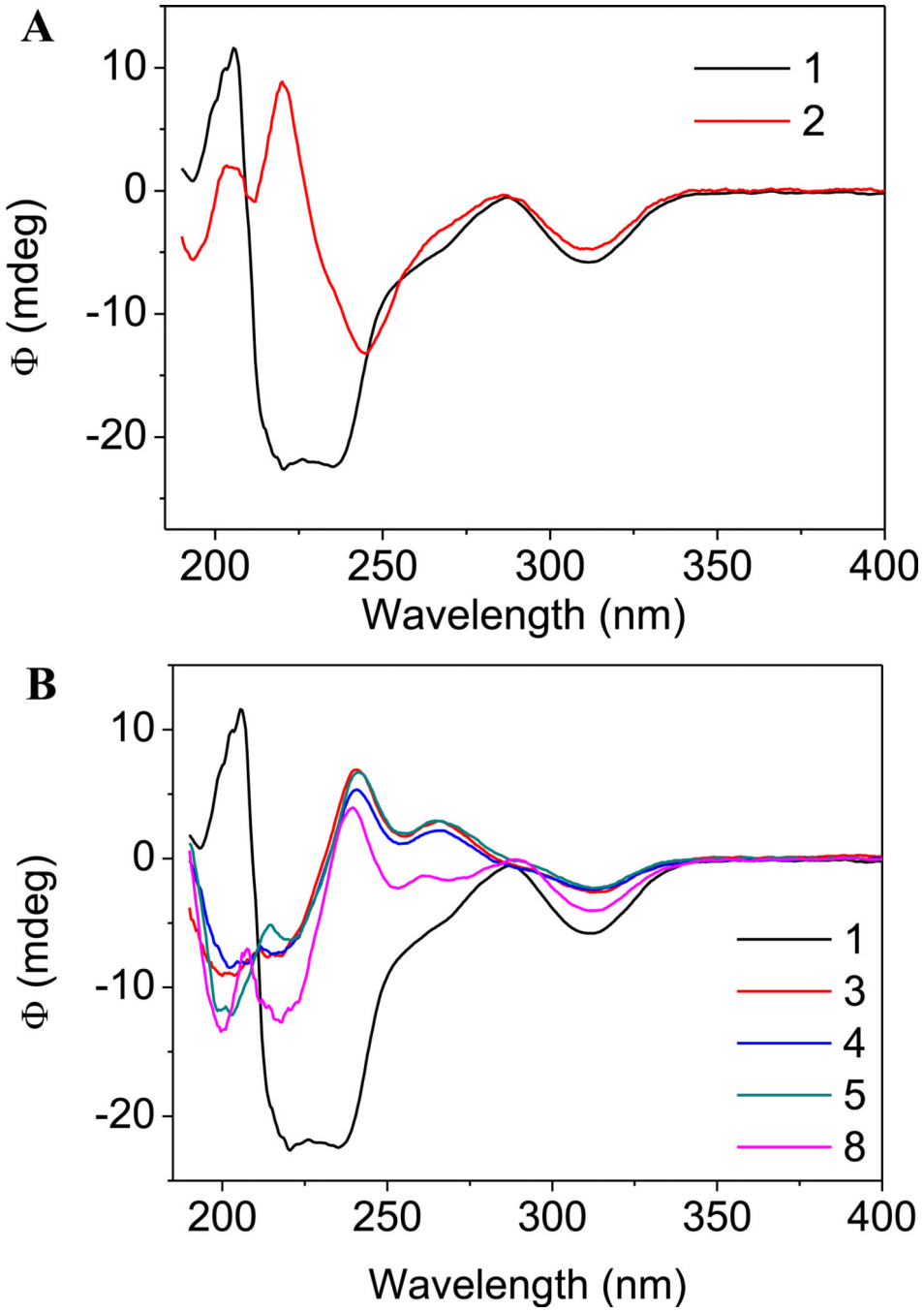

Fig. 2.

Panel A. CD spectra for natural noscapine **1** and its 9′-bromo derivative **2** in acetonitrile. Panel B. CD spectra for natural (−)-α-noscapine **1** and for representative novel 9′-alkyl and 9′-arylnoscapines in acetonitrile.

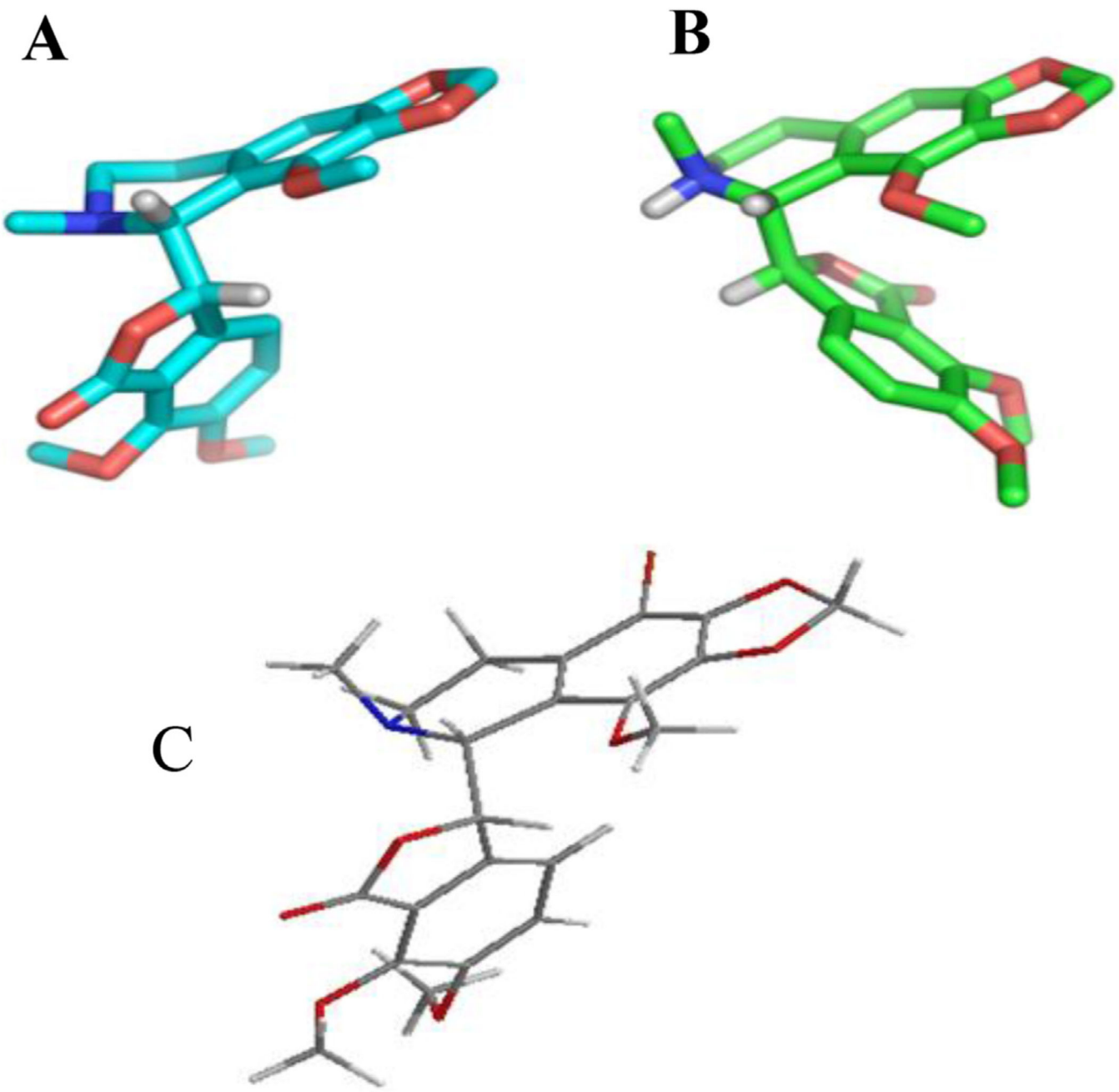

Fig. 3.

The X-ray crystal structures of natural noscapine free base (**1**, Panel A), its HCl salt (Panel B) and 9′-bromonoscapine (**2**, Panel C).

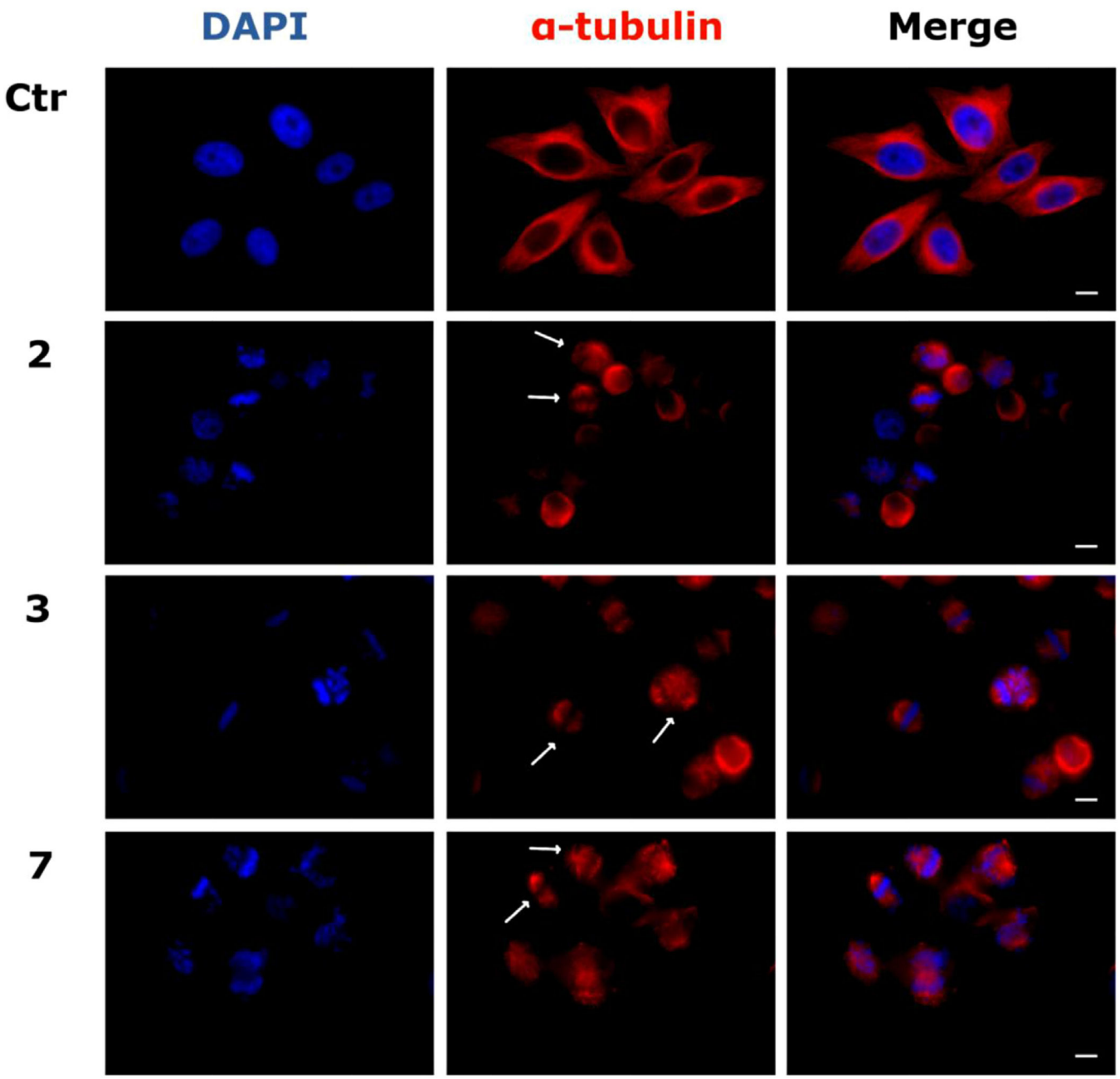

Fig. 4.

Effects of compounds **2, 3** and **7** on microtubule networks in HeLa cells. Cells were incubated with 25 μM compound for 24 h and then stained with anti-β-tubulin primary antibody and secondary Alexa-conjugated antibody and then observed by confocal microscopy (magnification 20×, bar = 10 μm). Cells were also counterstained with DAPI to visualize the nuclei. Arrows indicate cells with disorganized spherical arrangements of chromosomes or multipolar microtubules.

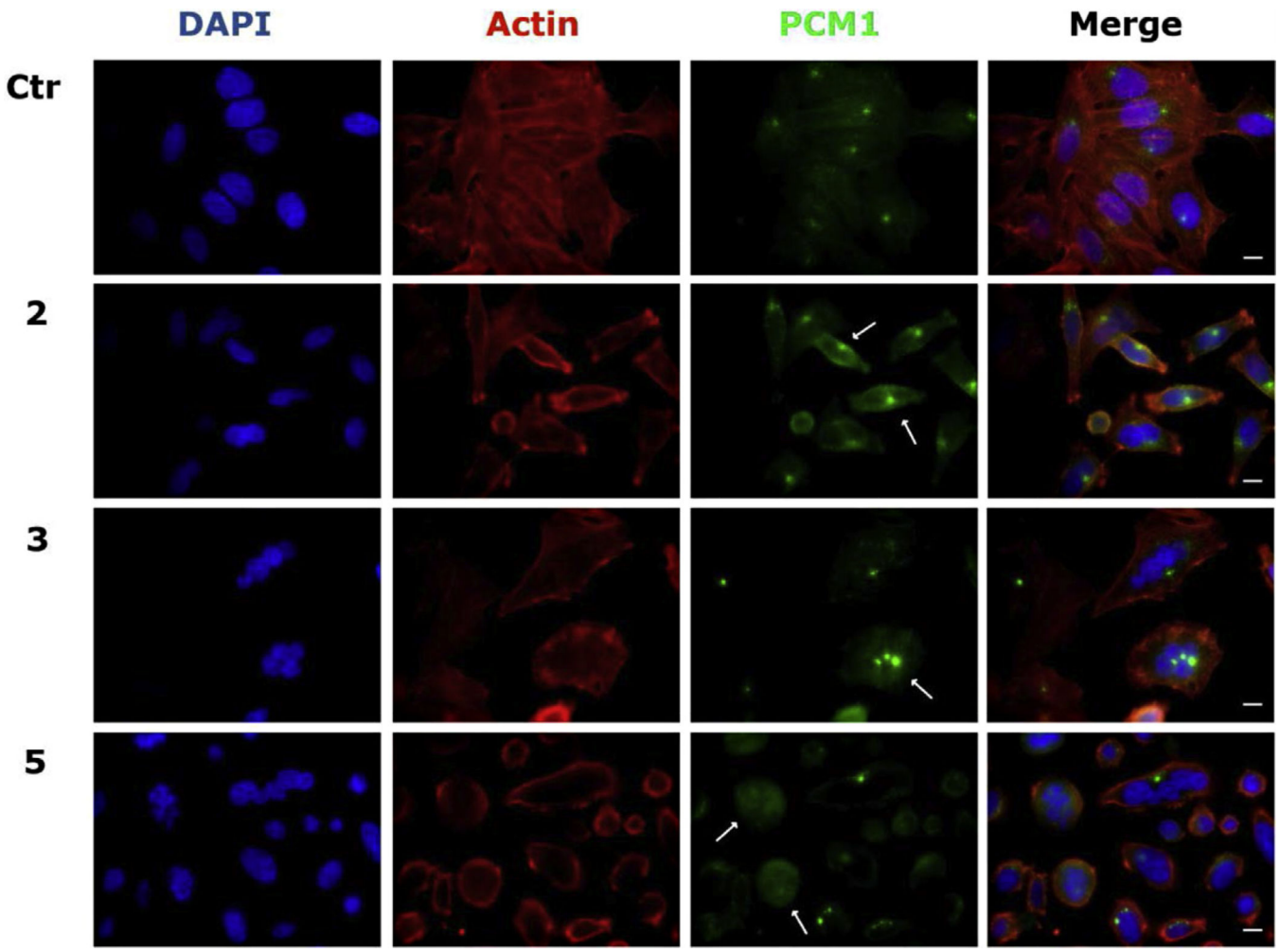

Fig. 5.

Effects of indicated compounds on PCM1 in HeLa cells. Cells were incubated for 24 h with the indicated compounds (25 μM) and stained with anti-PCM1-primary antibody and secondary Alexa-conjugated antibody, phalloidin-tetramethylrhodamine B to visualize actin microfilaments and DAPI. Images were captured by confocal microscopy (magnification 60×, bar = 10 μm). Arrows indicate points of PCM1 accumulation or diffused in mitotic cells.

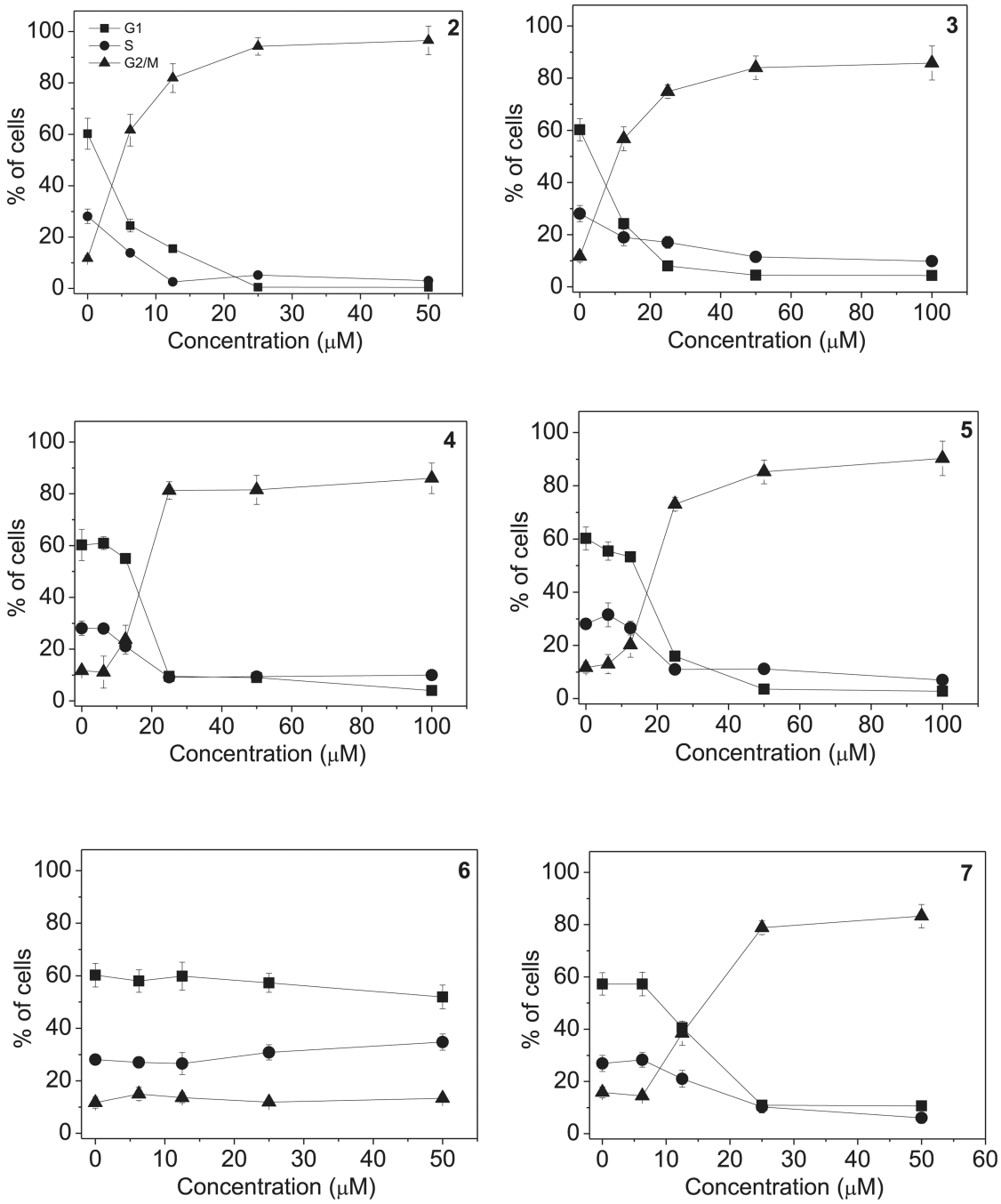

Fig. 6.

Percentage of cells in each phase of the cell cycle in HeLa cells, treated with the indicated compound at different concentrations for 24 h. Cells were fixed and labeled with PI and analyzed by flow cytometry as described in the experimental section. Data are presented as mean ± SEM of three independent experiments.

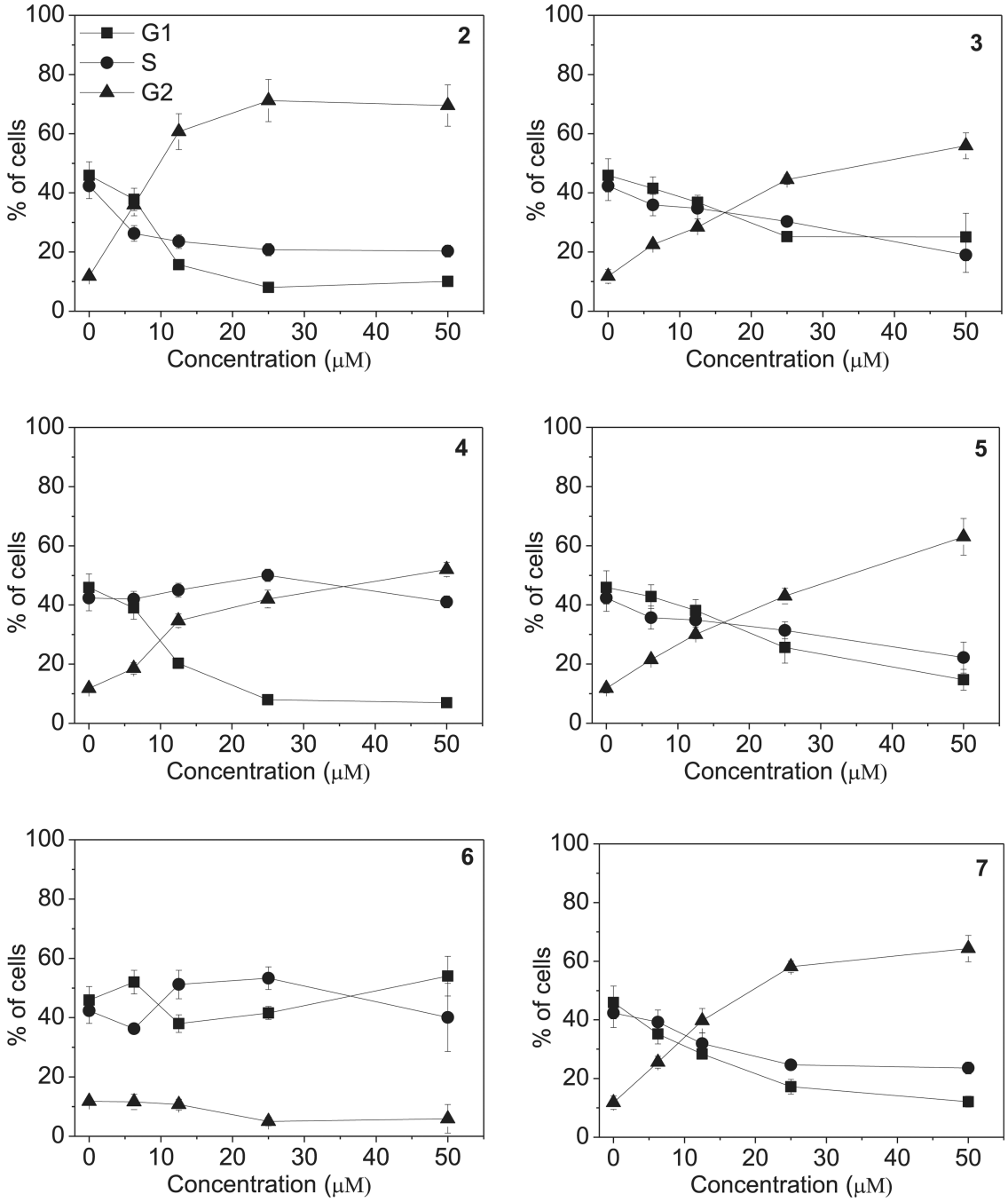

Fig. 7.

Percentage of cells in each phase of the cell cycle in Jurkat cells, treated with the indicated compound at different concentrations for 24 h. Cells were fixed and labeled with PI and analyzed by flow cytometry as described in the experimental section. Data are presented as mean ± SEM of three independent experiments.

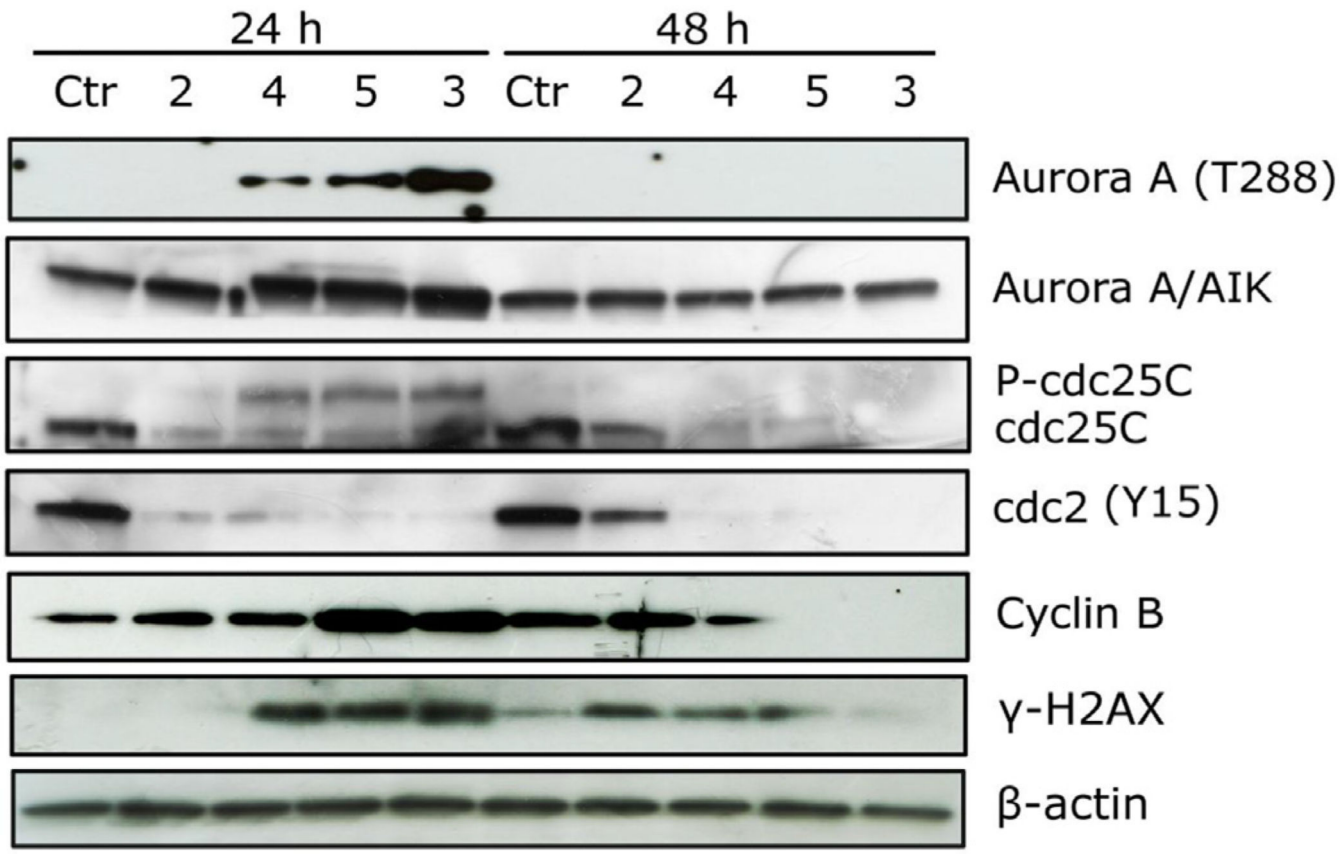

Fig. 8.

Effects of **2–5** on G2/M regulatory proteins. HeLa cells were treated for 24 or 48 h with the indicated compound at 25 μM. The cells were harvested and lysed for the detection of cyclin B, p-cdc2^{Y15}, cdc25C and γH2A.X expression by western blot analysis. To confirm equal protein loading, each membrane was stripped and reprobed with anti-β-actin antibody.

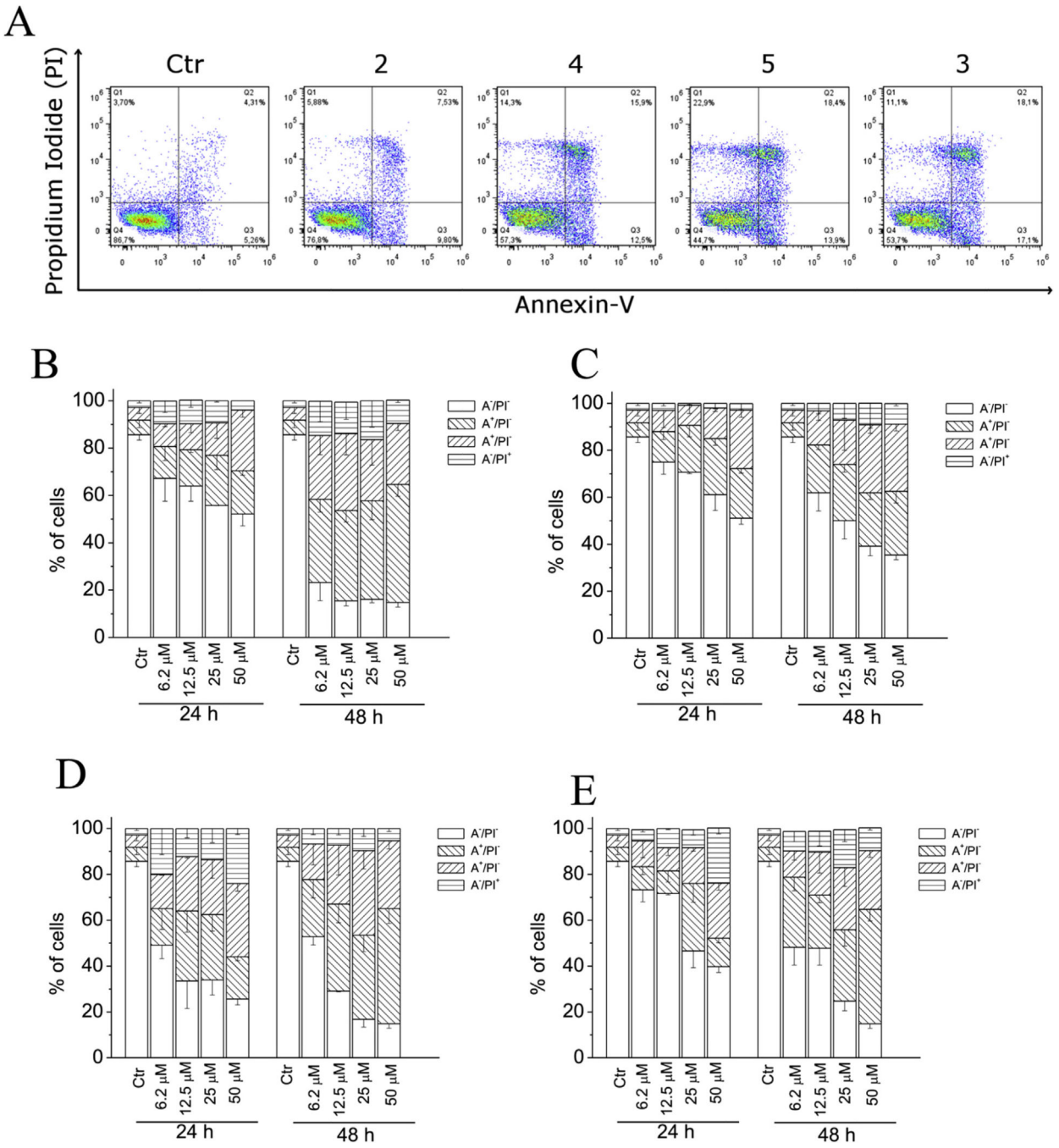

Fig. 9.

Flow cytometric demonstration of apoptosis by compounds **2, 3, 4** and **5**. A. Representative biparametric histograms obtained after a 24 h incubation of HeLa cells with the indicated compound at 25 μM. The cells were harvested and labeled with annexin-V-FITC and PI and analyzed by flow cytometry. In these histograms, the lower left-hand segment represents the annexin-V^-/PI^- cells, the lower right-hand segment the annexin-V^+/PI^- cells, the upper right-hand segment the annexin-V^+/PI^+ cells, and the upper left-hand segment the annexin-V^-/PI^+ cells. Percentage of cells found in the different regions of the biparametric

histograms shown in panel A and analogous histograms obtained after 48 h incubations are shown for compounds **2** (Panel B), **4** (panel C), **5** (panel D) or **3** (panel E) at the indicated concentrations. Data shown in panels B–E are presented as mean ± SEM of three independent experiments.

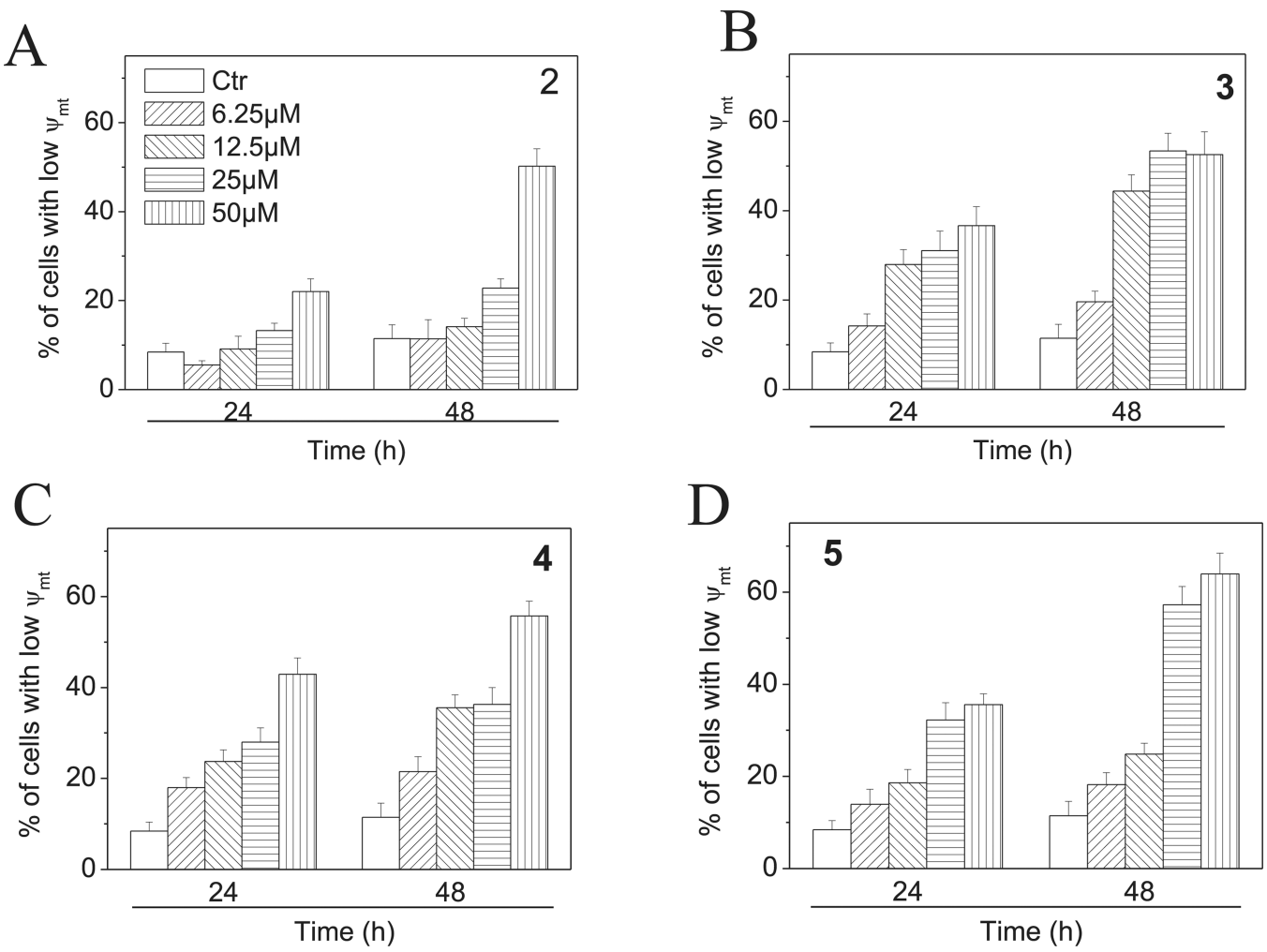

Fig. 10.

Assessment of mitochondrial membrane potential ($\Delta\psi_{mt}$) after treatment of HeLa cells with compounds **2–5**. Cells were treated with different concentration of the indicated compounds for 24 or 48 h and then stained with the fluorescent probe JC-1. Data are expressed as mean ± SEM for three independent experiments.

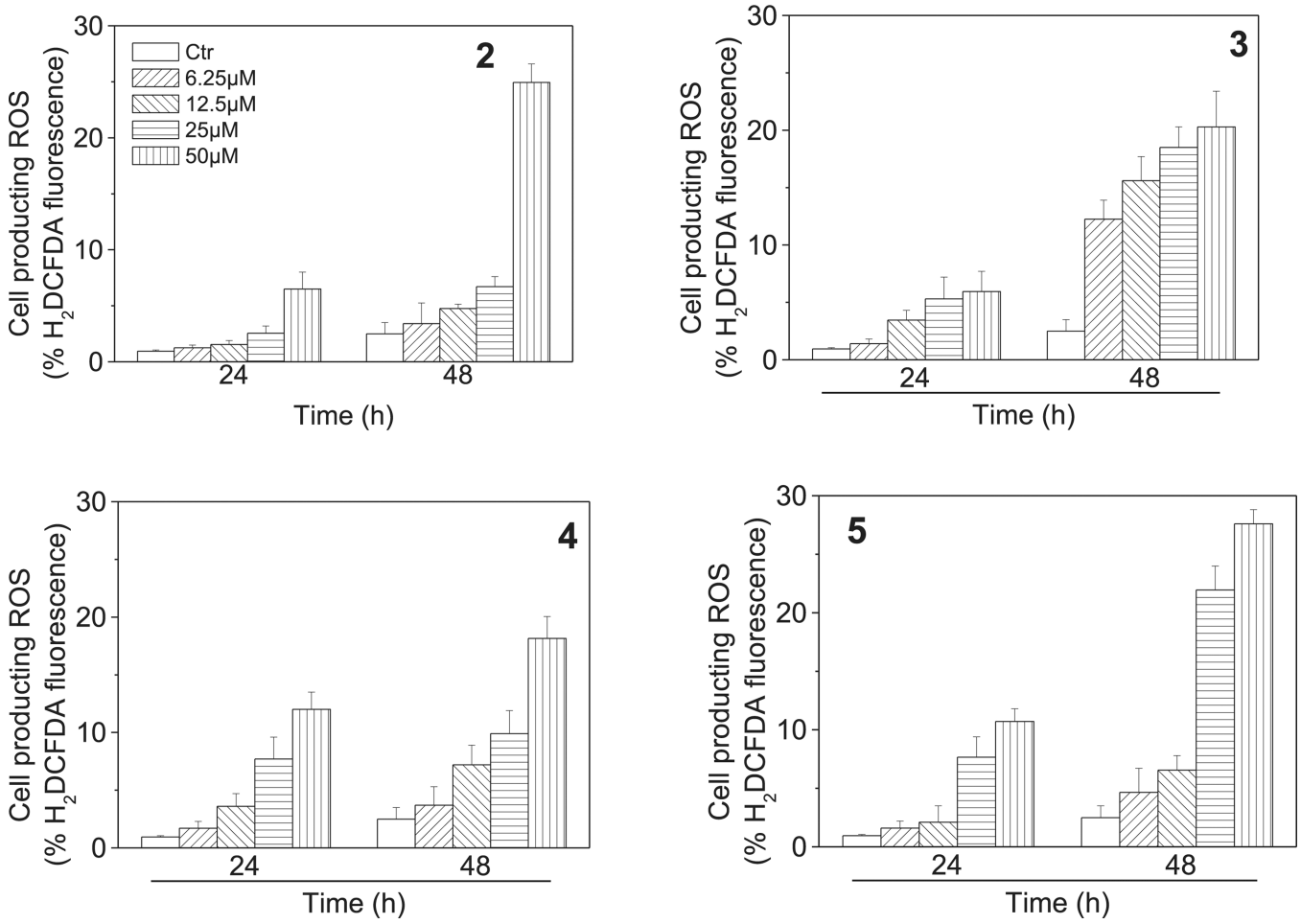

Fig. 11.

Mitochondrial production of ROS in HeLa cells following treatment with compounds **2–5**. After 24 or 48 h incubations with the indicated compounds at the indicated concentration, HeLa cells were stained with H2-DCFDA and analyzed by flow cytometry. Data are expressed as mean ± SEM of three independent experiments.

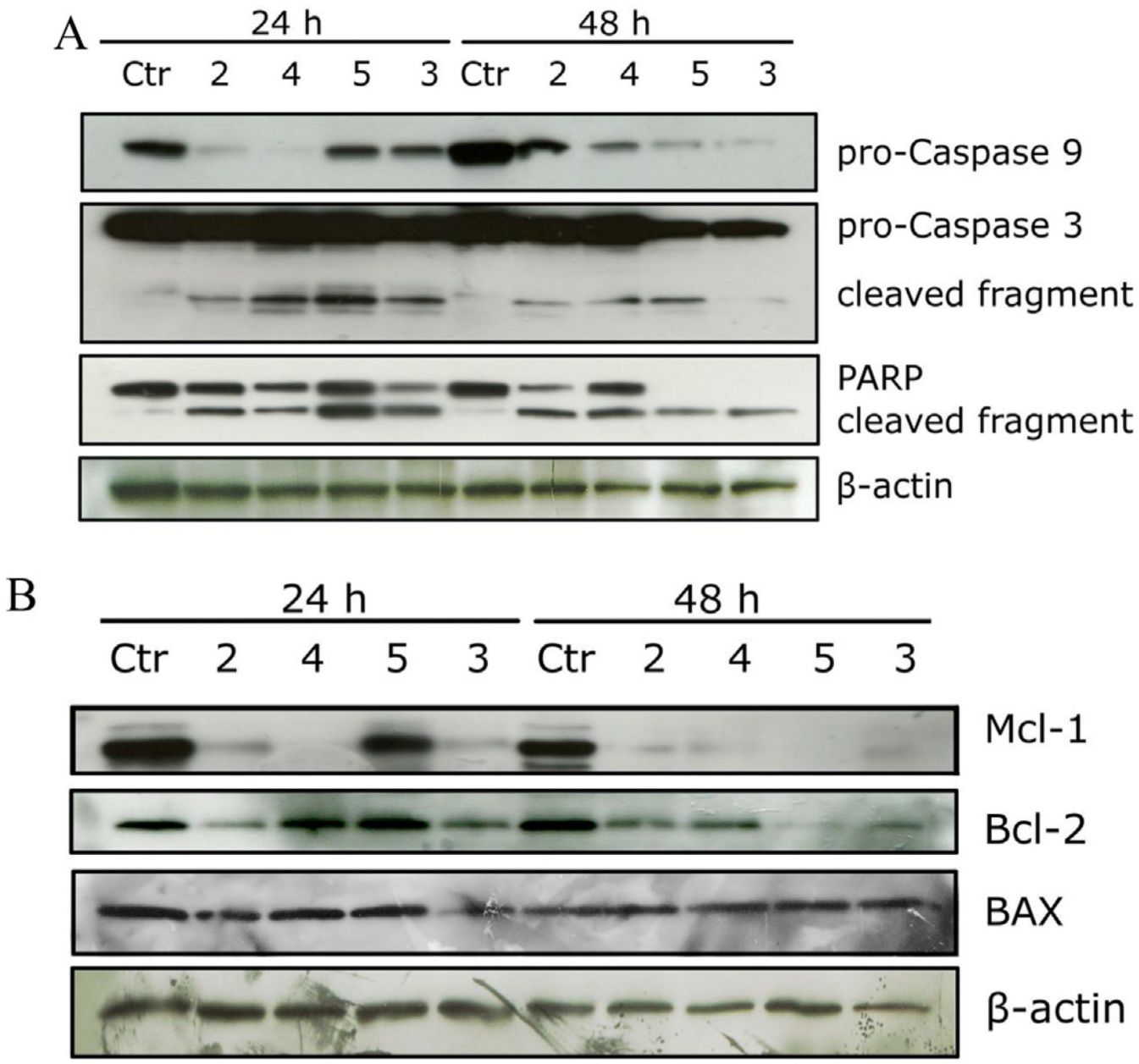

Fig. 12.

Effect of **2–5** on caspase activation (panel A) and on Bcl-2, Mcl-1 and Bax proteins (panel B) in HeLa cells. Cells were treated for 24 or 48 h with the indicated compounds at 25 μM. The cells were harvested and lysed for the detection of procaspase-9, pro-caspase-3, PARP, Mcl-1, Bcl-2 and Bax expression by western blot analysis. To confirm equal protein loading, each membrane was stripped and reprobed with anti-β-actin antibody.

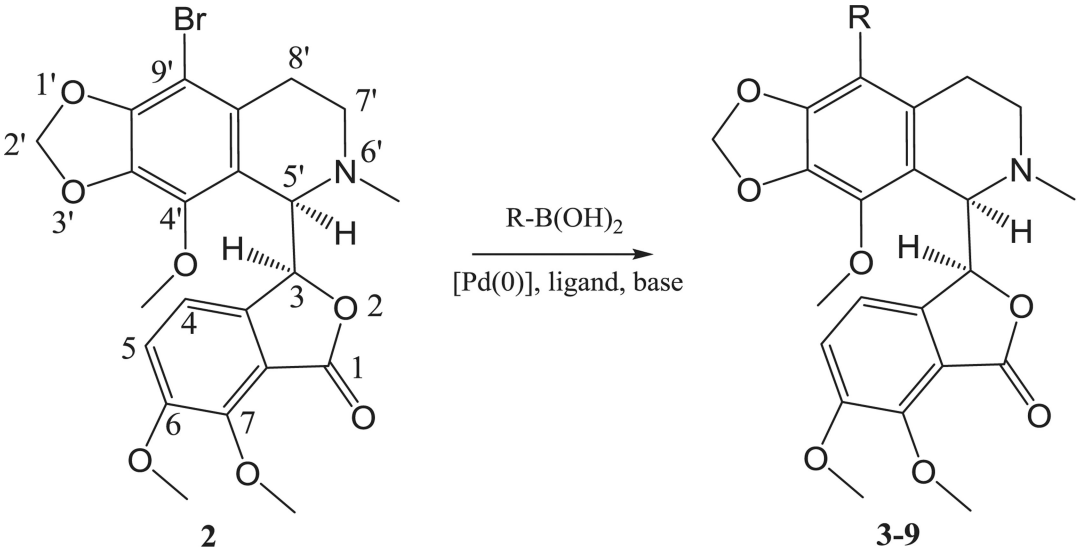

	R
3	Me
4	Ph
5	4-Me-Ph
6	2-OMe-Ph
7	3-OMe-Ph
8	4-OMe-Ph
9	2-naphthyl

Scheme 1.
Synthesis of targeted 9′-alkyl- and arylnoscapines **3–9**.

Table 1

Optimization of the Suzuki coupling of compound **2**.

Compounds	Pd-source	Ligand	Base	Solvents	Yields (%)
3	$Pd[P(Ph)_3]_4$	–	K_2CO_3	THF/MeOH	4
3	$Pd(OAc)_2$	XPhos[a]	K_3PO_4	THF/MeOH	44
4	$Pd[P(Ph)_3]_4$	–	K_2CO_3	THF/MeOH	12
4	$Pd(OAc)_2$	Xphos[a]	K_3PO_4	THF/MeOH	53
5	$Pd[P(Ph)_3]_4$	–	K_2CO_3	THF/MeOH	8
5	$Pd(OAc)_2$	Xphos[a]	K_3PO_4	THF/MeOH	61
6	$Pd[P(Ph)_3]_4$	–	K_2CO_3	THF/MeOH	4
6	$Pd(OAc)_2$	XPhos[a]	K_3PO_4	THF/MeOH	41
7	$Pd[P(Ph)_3]_4$	–	K_2CO_3	THF/MeOH	9
7	$Pd(OAc)_2$	Xphos[a]	K_3PO_4	THF/MeOH	55
8	$Pd[P(Ph)_3]_4$	–	K_2CO_3	THF/MeOH	4
8	$Pd(OAc)_2$	XPhos[a]	K_3PO_4	THF/MeOH	42
9	$Pd[P(Ph)_3]_4$	–	K_2CO_3	THF/MeOH	7
9	$Pd(OAc)_2$	Xphos[a]	K_3PO_4	THF/MeOH	57

[a]XPhos: (2-biphenylyl)-dicyclohexyl-phosphine.

Table 2

In vitro cell growth inhibitory effects of compounds **2**–**9**.

IC_{50}[a] (μM)									
Compounds	**HeLa**	**Jurkat**	**SEM**	**RS4; 11**	**CEM**	**LoVo**	**HT29**	**A549**	**IGROV-1**
2	2.6 ± 0.4	3.0 ± 0.6	1.8 ± 0.3	1.4 ± 0.6	2.8 ± 0.19	42.8 ± 16.7	18.7 ± 7.0	73.9 ± 7.6	78.2 ± 6.9
3	5.2 ± 0.8	5.9 ± 0.8	4.3 ± 0.7	15.8 ± 2.0	8.8 ± 3.1	66.3 ± 10.1	34.0 ± 10.4	>100	62.4 ± 3.5
4	7.4 ± 1.6	5.4 ± 2.1	3.2 ± 0.4	2.4 ± 0.7	5.2 ± 0.8	42.8 ± 2.8	36.5 ± 7.1	55.3 ± 3.2	68.1 ± 6.1
5	12.8 ± 3.8	5.1 ± 0.9	7.4 ± 1.1	16.4 ± 3.5	11.8 ± 2.2	41.8 ± 3.6	24.9 ± 7.3	22.2 ± 7.9	66.3 ± 7.3
6	30.8 ± 1.9	33.6 ± 5.1	22.2 ± 3.2	13.8 ± 5.4	6.9 ± 1.5	57.1 ± 4.4	72.7 ± 12.0	59.7 ± 5.3	90.9 ± 11.7
7	8.9 ± 0.3	13.2 ± 4.2	13.0 ± 4.0	7.1 ± 2.9	22.3 ± 4.7	29.4 ± 2.7	36.1 ± 5.8	>100	57.2 ± 9.3
8	15.6 ± 5.3	11.3 ± 4.7	15.1 ± 3.9	12.6 ± 1.9	25.8 ± 1.7	28.8 ± 1.5	47.8 ± 4.2	>100	55.6 ± 2.8
9	27.4 ± 3.5	20.0 ± 4.7	8.4 ± 2.1	30.8 ± 0.9	23.3 ± 3.4	60.3 ± 4.5	58.5 ± 10.3	48.1 ± 6.2	67.0 ± 8.4

[a] IC_{50} = compound concentration required to inhibit tumor cell proliferation by 50%. Data are presented as the mean ± SEM from the dose–response curves of at least three independent experiments.

Table 3

Cytotoxicity of noscapine derivatives for human peripheral blood lymphocytes (PBL).

Compound	IC_{50} (μM)[a]	
	$PBL_{resting}$ [b]	PBL_{PHA} [c]
2	>200	92.2 ± 13.8
3	>200	>200
4	>200	54.9 ± 7.6
5	>200	>200
6	>200	42.4 ± 5.0
7	>200	>200
8	>200	>200
9	>200	>200

[a] Compound concentration required to reduce cell growth by 50%.

[b] PBL not stimulated with PHA.

[c] PBL stimulated with PHA. Values are the mean ± SEM for three separate experiments.

Table 4

Inhibition of tubulin polymerization and colchicine binding by compounds **1**–**7** and CA-4.

Compound	Tubulin assembly[a] IC_{50} ± S.D (μM)		Colchicine binding[b] % ±S.D.	
	Extent	Rate	5 μM drug	500 μM drug
1	>400	170 ± 4	n.s.	44 ± 4
2	>400	>400	n.s.	34 ± 4[c]
3	>400	220 ± 50	n.s.	39 ± 2[c]
4	>400	>400	n.s.	14 ± 1[c]
5	120 ± 3	45 ± 8	n.s.	64 ± 4
6	>400	>400	n.s.	13 ± 5[c]
7	>400	170 ± 20	n.s.	38 ± 4
CA-4	1.2 ± 0.09	0.44 ± 0.03	99 ± 0.4	n.d.

[a] Inhibition of tubulin polymerization. Tubulin was at 10 μM.

[b] Inhibition of [^{3}H]colchicine binding. Tubulin and colchicine were at 1 and 5 μM, respectively, and the tested compound was at the indicated concentration. n.s., not shown, and n.d., not determined.

[c] In the indicated samples, turbidity was observed in the reaction mixtures, implying compound precipitation and a saturating, but unknown, concentration of the added compound.